5 Specialized SEM Techniques

This chapter describes various imaging techniques used in the SEM. Some of these techniques require specialized equipment, devices, or detectors, while others are simply accomplished by manipulating standard operational parameters available with the SEM. The techniques discussed in this chapter include imaging at low voltage and low vacuum, focused ion beam (FIB), STEM-in-SEM, electron backscatter diffraction (EBSD), electron beam lithography, electron beam-induced deposition (EBID), and cathodoluminescence.

5.1 Imaging at Low Voltage

The two types of secondary electron signals obtained from a specimen can be designated as SE_1 and SE_2. The secondary electrons SE_1 are produced within the narrow escape depth of the specimen and are localized within a few nanometers of the impinging electron beam. These electrons make up the high-resolution image as they correspond to local fine features. Secondary electrons SE_2 are produced by the backscattered electrons that inelastically scatter secondary electrons which in turn emanate from the specimen surface. These secondary electrons carry a low-resolution signal. Similarly, those backscattered electrons that emanate from the immediate vicinity of the incident beam and have lost minimal of incident energy form high-resolution backscattered signal. A high-resolution image is obtained by separating the high-resolution SE and BSE signals from low-resolution SE and BSE signals, respectively. One way to achieve that is to undertake imaging at low accelerating voltages ranging from 0.1 to 5 kV. At high accelerating voltage (i.e., 15–30 kV), the signal is derived from larger depths of the specimen which tends to obscure surface features. As the beam energy is lowered, the specimen interaction volume decreases sharply resulting in a high-resolution high contrast SE and BSE signal emanating from fine features close to the specimen surface giving rise to images with greater surface detail. Due to the small interaction volume generated at

© Springer Nature Switzerland AG 2018, Corrected Publication 2023

A. Ul-Hamid, *A Beginners' Guide to Scanning Electron Microscopy*,
https://doi.org/10.1007/978-3-319-98482-7_5

low kV, both SE and BSE signals produced are of a high spatial resolution giving rise to stronger image contrast. Production of low-resolution signals such as SE_2, SE_3, and BSE farther away from the probe is eliminated. Effects of specimen charging and edge brightness are also reduced at low beam energies. This imaging technique is also suitable for beam-sensitive specimens as it minimizes radiation damage.

However, use of low voltage during imaging is not free of challenges (also see Sect. 4.1.2.4). Disadvantages of this technique include decreased gun brightness, increased chromatic aberration (see Eq. 2.10), increased diffraction contribution at the aperture (see Eq. 2.11), and contamination buildup relative to the low depths from which the signals are generated. Low-energy beams are also susceptible to electromagnetic interference effects. If the beam current and gun brightness are kept constant, operation at low kV results in a significantly larger spot size resulting in decreased resolution. The brightness of gun source decreases due to lowered accelerating voltage; however, signal-to-noise ratio remains solid down to 500 V due to an increased SE signal. Use of high brightness source with low energy spread, and an immersion lens typically used in the modern field emission microscopes helps to maintain reasonable image contrast and provide surface-sensitive information. Cold field emitters are also least affected from *Boersch effect* [1] (e.g., defocusing at crossover) due to low beam current employed in this type of gun. It is advisable to employ short working distance during imaging at low voltages to mitigate the effects of lens aberrations and any extraneous electromagnetic field present in the work environment. Images taken at low beam energy appear *flatter* (less 3-D like) and translucent (less solid). Compositional (Z) contrast is also less evident. The usual practice is to undertake BSE imaging at low voltages to avoid charging effects, although the images tend to be slightly noisy. The rate of contamination buildup can be reduced by avoiding high magnification, by focusing and removing astigmatism in an area other than that used for imaging, and by not using spot or reduced area raster mode. Clean specimen chamber with high-quality vacuum system, stable and vibration-free platform and proper shielding from electromagnetic influences has enabled imaging at a few tens of volts. Example of images taken at three different accelerating voltages is shown in Fig. 4.8a-c.

5.1.1 Electron Energy Filtering

Various advanced techniques have been developed for low voltage imaging [2, 3]. One approach is to use energy filtering of the signal that enters the in-lens or through-the-lens (TTL) detector present in the SEM that is equipped with field emission gun and an immersion lens. The field emission source and advanced optics serve to achieve a probe at nanometer scale, while the filter works to separate the low-energy SE from the high-energy SE and BSE. The final image can be selected to compose of mainly SE or BSE or combination of both depending on the detected signal. Two types of filters are used in commercial SEMs. One employs a control

electrode with an E × B filter (developed by Hitachi High-Technologies) [4, 5], and the other is known as r-filter (JEOL Ltd.) [6].

5.1.1.1 E × B Filter

The control electrode is located within the objective lens in the SEM column below the upper detector. Conversion electrode and E × B filter (Wien filter) are positioned in the column above the control electrode (see Fig. 5.1a). E × B filter has electrostatic and magnetic field crossed at right angles to the trajectory of SE. When the control electrode is positively biased, low- and high-energy SE enter the detector and line-of-sight BSE strike the conversion electrode to emit SE which then enter the detector. When the control electrode is negative (see Fig. 5.1b), low-energy SE can be rejected, or its detection can be controlled in combination with BSE by regulating the extent of negative bias on the control electrode. Low-energy SE are primarily responsible for charging effects. The ability to filter low energy from the high energy signal enables better control during low voltage imaging.

BSE to SE conversion occurs at a large solid angle of collection. The SE yield for each backscattered electron that strikes the conversion electrode actually increases at low accelerating voltages, making this technique quite useful for low voltage imaging. The SE signal generated in this manner contains information about the BSE emanating from the specimen.

5.1.1.2 r-Filter

In this technique, a cylindrical conversion electrode is placed within the objective lens as shown in Fig. 5.2. The voltage applied to the electrode produces an electric field which deflects the electrons of certain energy and eliminates them through collision with cylinder walls. In this manner, the signal to the detector can be continuously controlled by regulating the voltage applied to the electrode. This serves to “filter” the signal on the basis of energy and can be used to create SE or BSE image or a combination of both. Figure 5.3a, b shows images taken using r-filter technology.

5.1.2 Detector Technology

5.1.2.1 Energy Selective Backscatter (EsB) Detector (Made by Zeiss)

Energy filter can be made part of the detector. Zeiss has manufactured an in-lens scintillator detector with a filter attached to its front end for its GEMINI SEM column. It is called EsB (energy selective backscatter) detector and is located above the in-lens SE detector [7, 8]. It is used to create BSE images. The filtering grid fixed at the front of the detector is set at 0 to −3 keV potential that repels low-energy SE and allows only BSE to pass through to the detector.

5.1.2.2 Upper Electron Detector, UED (Made by JEOL Ltd)

A set of two detectors can be used in the column. The filter attached to the upper detector is set at a potential, for example, −300 V. Electrons with kinetic energy

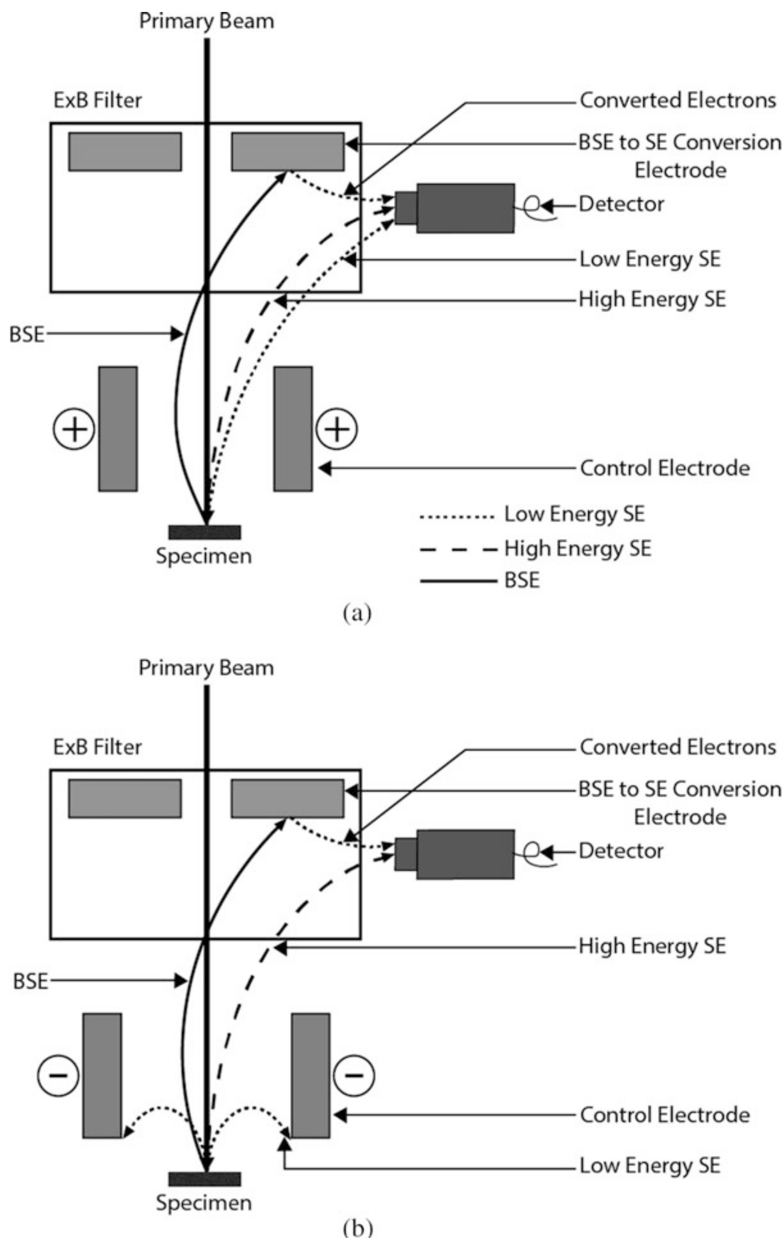

Fig. 5.1 Schematic showing energy-filtering techniques that consist of a control electrode and an $E \times B$ filter that has electrostatic and magnetic fields perpendicular to the incoming SE signal. (**a**) When the control electrode is positively biased, low and high-energy SE enter the detector. Line-of-sight BSE strike the conversion electrode to generate SE which are also directed into the detector. (**b**) When the control electrode is negative, low-energy SE are rejected, while high-energy SE and BSE are detected. The magnitude of negative bias on the control electrode can be regulated to determine the energy range of the electrons that are detected

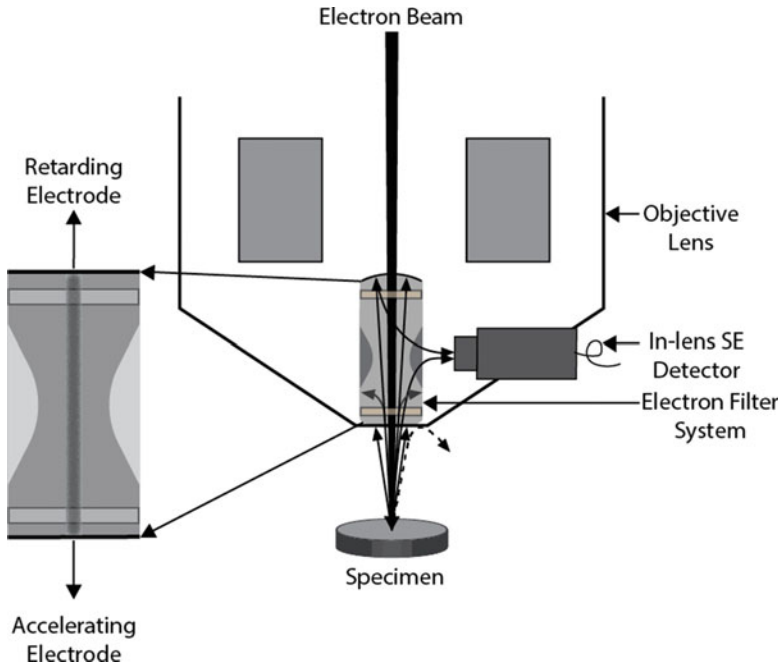

Fig. 5.2 Schematic showing r-filter technology where cylindrical conversion electrode placed within the objective lens deflects the electrons within a selected energy range and eliminates them through collision with cylinder walls. The signal is thus filtered based on electron energy and is used to create SE or BSE image or a combination of both

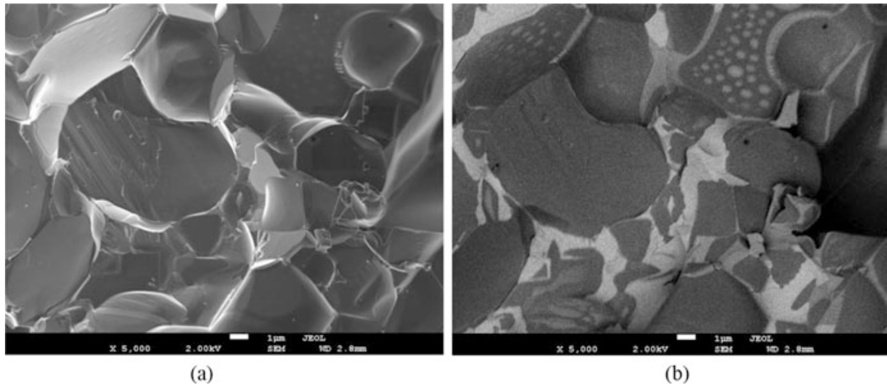

(a) (b)

Fig. 5.3 SEM images of fractured Al alloy surface obtained at an accelerating voltage of 2 kV and a working distance of 2.8 mm, showing the capability of r-filter developed for energy filtering. (**a**) SE image formed predominantly by SE showing clear surface details and (**b**) BSE image formed using primarily BSE showing the presence of a distinct phase (light gray contrast) within Al grains. Note the surface details within Al grains are relatively obscured in this image

>300 V will pass through and be detected by upper electron detector (UED) [9]. Electrons with lesser kinetic energy will not pass through and get deflected to be detected by the other SE detector. The images obtained in this manner will show different levels of specimen surface details.

5.1.2.3 Solid-State Backscattered Detector

Use of a solid-state semiconductor detector is usually not suitable for low voltage imaging as the signal emanating from the specimen has to pass through surface electrode and Si dead layer before it can reach the active detector surface. This results in loss of energy of the order of 2–5 keV in the signal. This energy threshold clearly implies that low-energy electrons typically ejected from the specimen during low voltage microscopy cannot be detected with a solid-state detector.

However, recent developments have seen the advent of novel backscattered detectors that employ ultrathin doped layer that allows low-energy electrons to pass through. FEI® has developed an annular detector with eight segments that allows detection of BSE emanated from the specimen at various angles [10, 11]. The segments can be used selectively to use specific electrons for the formation of the final image. This detector is called distributed backscattered (DBS) detector. It can be used in either concentric backscattered mode or angular backscattered mode allowing specific information to be obtained from the specimen.

JEOL Ltd. has also developed a retractable low-angle backscattered electron (LABe) detector which can be used as a conventional BSE detector at large working distances and intermediate accelerating voltages to collect high-angle BSE [12, 13]. It can also be employed at a very short working distance where it collects low-angle BSE at low accelerating voltage. In the latter case, it provides surface-sensitive information. This detector can be used in conjunction with beam deceleration with final landing energies of few hundred volts only, which makes it highly suitable for imaging charging samples.

5.1.3 Electron Beam Deceleration

As mentioned earlier, there are some disadvantages associated with the use of low accelerating voltage during imaging. Unlike at high beam energy, space charge within the SEM column is not negligible during low voltage operation. Gun emission current is low, energy spread of the beam is large, and crossover diameter is increased due to Coulomb interaction between the electrons known as the *Boersch* effect. This becomes a serious issue especially at low beam energies of around 1 kV. An additional extractor electrode incorporated in the gun design helps mitigate these effects. Another advancement to overcome the drawbacks of low voltage imaging has been the introduction of *beam deceleration* [14]. In this technique, the electron beam is kept at high energy as it passes through the SEM column. Once it exits the final lens, the beam is decelerated before it strikes the specimen surface. By maintaining the beam at high energy during its movement through the column and lenses, large energy spread, *Boersch* effect, and chromatic aberrations are avoided.

The beam lands on the specimen surface with lesser energy which serves to reduce beam penetration and interaction volume. Beam deceleration technique manages to inhibit specimen charge-up by reducing landing energy significantly. With this technique, greater flexibility in the selection of beam voltages becomes available. It enables detection of electrons scattered at shallow depths emphasizing its surface features. It improves microscope resolution and contrast at low accelerating voltages. Beam deceleration is a relatively simple technique that can be incorporated within the existing electron sources and columns eliminating the need for a separate SEM system.

Beam deceleration is accomplished by applying a negative bias (up to −4 kV) to the stage which sets up an electric field between the specimen and the detector, acting as an additional electrostatic lens working to retard the beam accelerating voltage immediately before it hits the specimen. The energy with which the beam lands onto the specimen surface is known as *landing energy* and is equal to accelerating voltage minus stage bias. The landing energy can be controlled by varying the electron gun voltage and stage bias to achieve the optimum imaging quality. Since the beam is confined to a small surface area on the specimen, the effect of stray magnetic fields on imaging is also curbed. The electric field generated on the specimen surface due to stage bias tends to counter small electric fields that may otherwise exist at the sample surface under usual imaging conditions. This serves to minimize effects such as streaking and any possible disruptions to the trajectories of electrons emitted from the specimen. In addition, emitted secondary electrons are accelerated during beam deceleration, which increases signal collection efficiency. The specimen, however, needs to be flat to be able to remain unaffected by the strong electric field created at its surface. For rough, tilted, or composite samples consisting of conductive and insulating material, complex electric fields generated at the specimen surface may render the use of beam deceleration technique less viable.

Beam deceleration can be used with both backscattered and secondary electron detectors. However, backscattered detectors are more suitable, while the standard E-T detector is less efficient. SEM images shown in Fig. 5.4a, b reveal the benefit of beam deceleration technique. It can be seen that surface details are clearly visible without any charging effects in Fig. 5.4b. Figure 5.4c–f show SE and BSE images of uncoated nonconductive toner cartridge particle and paper samples obtained at various landing energies of 300–2000 eV. It can be seen that surface details are visible without significant charge-up.

5.1.4 Recent Developments

Aberration correctors have been developed for SEM, and this technology has seen great improvements in the last decade. Multipole aberration correctors are used to minimize chromatic and spherical lens aberrations in microscopes equipped with cold field emission guns [15–20]. Despite remarkable technological advancement, their use is presently cumbersome and puts limitations on the depth of field and size and shape of the specimen that can be examined. Nevertheless, aberration correction

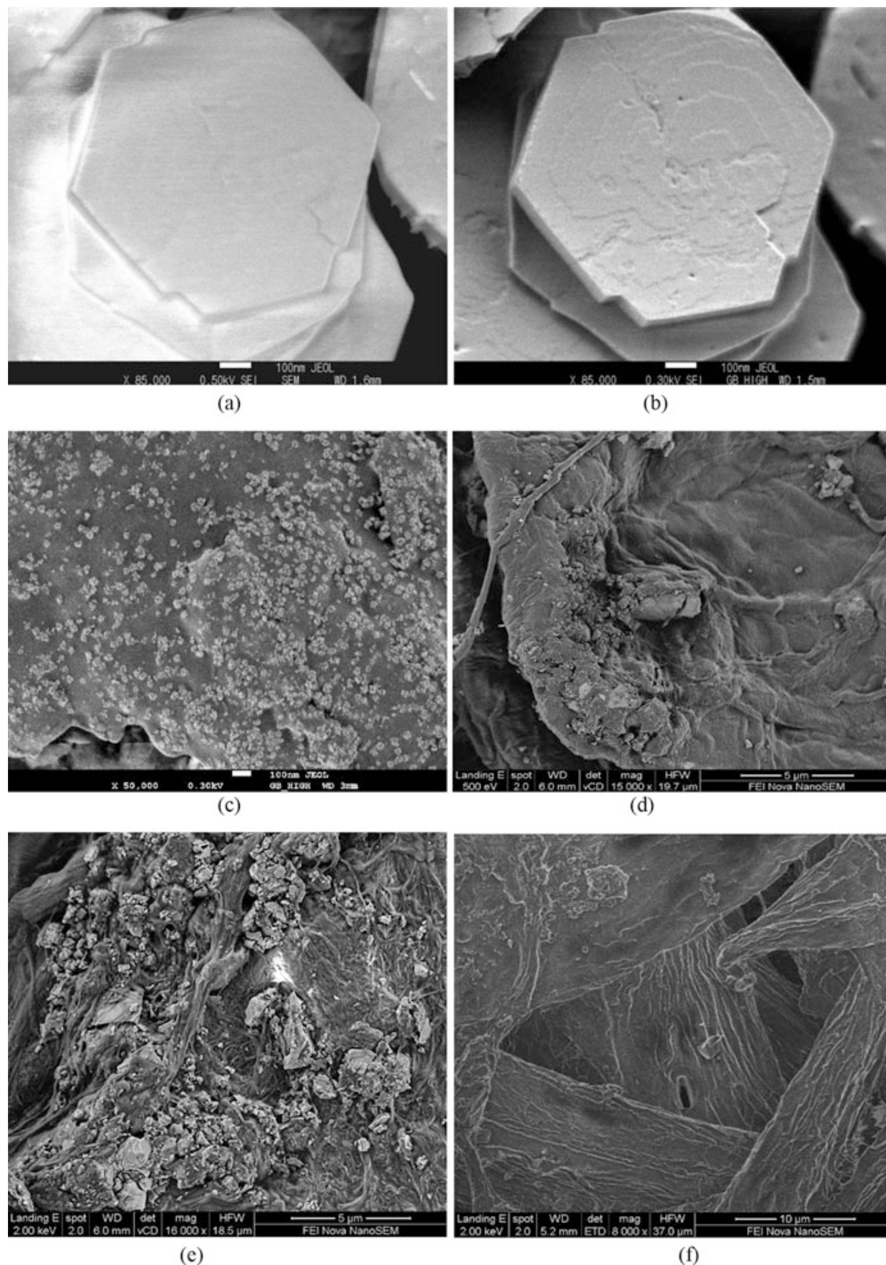

Fig. 5.4 Use of beam deceleration technique enables imaging of nonconductive materials at high magnification without any significant charge-up. High magnification secondary electron image at (**a**) 500 V and (**b**) 300 V. The latter image shows more surface details. (**c**) Backscattered SEM image of toner cartridge sample. Landing energy is 300 V. (**d**, **e**) Backscattered SEM images of paper at landing energies of 500 and 2,000 eV, respectively. (**f**) Secondary electron image of paper at landing energy of 2 keV

technology is expected to improve steadily in the future and overcome these drawbacks.

An advanced design suitable for low voltage imaging consists of an electron source that is immersed within the electromagnetic field of low aberration condenser lens and can produce 5 nm spot size with 5 nA current at an accelerating voltage of 3 kV. Present-day SEMs have demonstrated resolutions of 1.4 nm at 1 kV and 5 nm at 0.1 kV. Another important development in the field of low voltage imaging has been the introduction of a monochromator for field emission SEM. Such FE-SEM reduces the energy spread of Schottky field emission source to <0.2 eV, thus diminishing the influence of chromatic aberration. This makes imaging at low kV possible, without having to forego high current capabilities of Schottky field emitter [2, 3].

5.1.5 Applications

FE-SEM can be used to observe nanomaterials such as nanoparticles, nano-wires, and nanotubes by utilizing a STEM-in-SEM technique. This method reduces knock-on damage, compared to imaging with conventional high voltage TEM or STEM. Low kV FE-SEM can also be used to image layers of graphene deposited on Ni substrate. The lower rate of thermal damage at low kV also makes this technique suitable for beam-sensitive materials. By using a combination of reduced beam current and low kV, FE-SEM can be used to image semiconductor materials with high resolution and minimum damage.

5.2 Imaging at Low Vacuum

5.2.1 Introduction

In the normal working mode, specimen chamber is usually under high vacuum (e.g., 10^{-3} Pa or less). The high vacuum within the SEM column and specimen chamber ensures smooth travel of electron beam from the gun source to the specimen without getting scattered due to any residual gas molecules. Without an appreciable vacuum, beam electrons will be scattered by air molecules present in the chamber. The high vacuum also prevents oxidation damage to the electron gun. While these vacuum conditions are suitable for imaging dry specimens, they are unfavorable for examining wet and dirty samples. Such specimens serve to degrade vacuum or contaminate the specimen chamber under normal vacuum. In addition, an uncoated and nonconductive specimen can acquire electric charge due to impingement of the electron beam at its surface. A specimen is thought to be charged up if the number of incident beam electrons impinging upon the specimen is more than the specimen current i_{sp} flowing out and secondary and backscattered electrons emitted from the specimen. Due to its nonconductive nature, the specimen is unable to discharge the negative charge. This can cause contrast variation, beam instability, and image

distortion. In order to overcome these problems, SEMs capable of imaging damp, dirty, or insulating samples under low/degraded vacuum were invented. Depending on the manufacturer, these microscopes go by different names such as low vacuum SEM, variable pressure SEM, environmental SEM, nature SEM, etc.

5.2.2 Brief History

Development of such apparatus started before conventional electron microscopes were even commercialized. An arrangement for imaging liquids in conventional SEM was proposed by Thornley back in 1960 [21]. This was achieved by placing the sample between two carbon films, which prevent the liquid from evaporation, thus minimizing the contamination of vacuum present in the column and in the chamber. Further advancements in this field allowed researchers to vary the pressure in the chamber to simulate the natural environment without degrading the vacuum present in the chamber itself. The specimen chamber was converted into a substage by isolating it from the electron column with the help of pressure differential apertures [22]. Isolation of specimen chamber from the column allowed the researchers to achieve 1,000 times greater pressure as compared to the column while allowing electron gun to function and access the chamber normally. Achieving high pressure in the chamber and high vacuum in the column simultaneously is made possible by isolating both components from each other and providing a pumping system to each component. This isolation is undertaken with the help of small differential aperture or pressure-limiting aperture (PLA) placed below the objective lens, which serves to separate the vacuum in the SEM column from that in the specimen chamber (see Fig. 5.5a–c). The vacuum in the column remains high while that in the chamber can be degraded typically by 1,000×. Wet or nonconductive specimens that charge up can be imaged using SEM equipped with a low vacuum mode where the vacuum is intentionally degraded to a pressure of several hundred Pascal. Environmental SEM can operate with pressures as high as 3,000 Pa and at a high relative humidity (up to 100%) within the chamber.

5.2.3 Working Principle

In low vacuum mode, gas or water vapor is injected into the specimen chamber around the specimen surface area. High-energy electron beam penetrates the water vapor with some scatter and interacts with the specimen surface. Secondary and backscattered electrons emanating from the specimen strike the water molecules and produce secondary electrons which in turn produce more secondary electrons upon interaction with the surrounding water molecules. Water molecules are changed into positive ions as a result of this interaction with incident beam and secondary/backscattered electrons emerging from the specimen. Positive bias applied to a detector accelerates secondary electrons toward the detector, while positive ions are pushed toward the negatively charged areas on the specimen. Further ionization

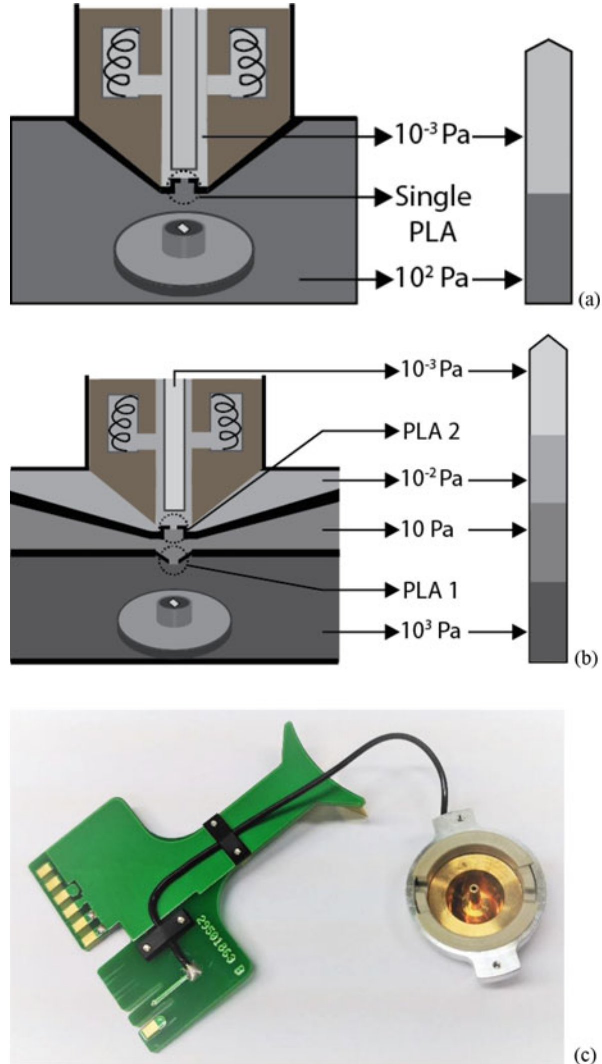

Fig. 5.5 The use of PLA allows maintaining a high vacuum within the column, while the vacuum in the chamber is degraded. (**a**) Schematic showing the use of pressure-limiting aperture (PLA) in SEM using low vacuum mode. (**b**) In another design, a combination of two PLA is used to degrade vacuum in the SEM chamber by an order of magnitude. (**c**) Photograph of PLA (seen protruding out) attached to low vacuum detector

events are produced due to this accelerated movement of electrons and ions. The water vapor thus serves to produce positive ions and also increases the number of secondary electrons resulting in gas amplification. Water vapor is a preferred choice for this application as it ionizes into positive ions easily. Generation of positive ions and their movement toward the negatively charged areas of the sample neutralize the negative charge accumulated at the specimen surface. This allows for charge-free imaging of nonconductive specimens without having to coat them with a conductive material. Another reason to use low vacuum can be to image moist or wet specimens such as clay or biological material. These samples can dry up under normal high vacuum and lose their features. Factors that affect the quality of imaging at low

vacuum include vapor pressure of the injected gas, working distance, accelerating voltage, spot size, and the area of the nonconductive surface.

Injection of water vapor in the SEM chamber serves the purpose of dissipating the charge buildup at the specimen surface. However, the components within the SEM electron column needs to be saved from water vapor and kept at high vacuum at all times. This is accomplished by inserting pressure-limiting aperture (PLA) beneath the objective pole piece at the point where the beam enters the chamber. This aperture is simply a disc with a small hole (shaped like a circular conical cylinder, see Fig. 5.5c). Since the pinhole has very small dimension, it is able to separate the two levels of vacuum without *interdiffusion* while allowing the beam to pass through. Any water vapor finding its way into the column is pumped out using oil diffusion or turbomolecular pump keeping the electron gun safe.

5.2.4 Detector for Low Vacuum Mode

Secondary electron image is usually not available in low vacuum mode because SE interacts with the water vapors immediately upon emitting from the specimen. Also, conventional E-T detector relies on a high bias (+10 kV) applied upon the scintillator to enable electron-to-photon conversion. Such high bias can easily ionize water vapor and arc the detector to ground. Thus, the use of E-T detector for SE imaging is ruled out, and BSE detector is generally employed to undertake BSE imaging. Use of BSE detector suffices as it is largely insensitive to the charging effect and produces images with good resolution. With the presence of gas particles in the chamber, special gas phase (large area scintillator) detectors are required for imaging. However, some manufacturers do provide special secondary electron detectors for use under low vacuum conditions.

The specialized gaseous detector, called gaseous secondary electron detector (GSED), (developed by Thermo Fisher Scientific) is used to undertake imaging with secondary electrons. This SE detector suitable for operation in a low vacuum is a positively biased electrode (see Fig. 5.6). It is mounted on the objective pole piece and can be dismounted after use. The positive bias of up to +600 V is applied on the GSED to attract secondary electrons. Due to gas amplification, the current collected by the detector is hundreds or even thousands times greater than the original signal. The detector is also placed closer (a few mm) to the specimen compared to an E-T detector, thus collecting SE efficiently. Positive bias on GSED also drives positively ionized water molecules toward the specimen to effectively neutralize the accumulated negative charge at specimen surface.

The advantage of using GSED in low vacuum mode is that specimen can be imaged in its original state without coating with gold or palladium. Images are free of distortions or contrast variations that commonly occur due to charging effects. Pits and voids at the specimen surface show better contrast as lack of charging allows electrons to eject out of the depths of the deep holes. GSED is not sensitive to light and therefore can be used to image specimens at high temperatures. Also, wet specimens can be examined.

Fig. 5.6 Schematic of gaseous secondary electron detector (GSED) with a central bore

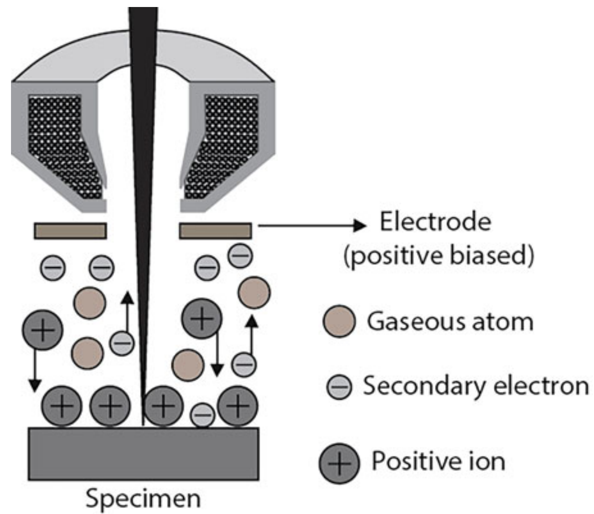

A conical pressure-limiting aperture is provided at the center of the detector to sustain low vacuum in the chamber while maintaining a high vacuum in the electron column. The smaller the bore size in the center of the GSED, the higher is the pressure that can be maintained in the specimen chamber. For instance, one-half of a millimeter can support a pressure of 1.3 kPa. Large field-of-view GSED with 1 mm bore size is also available. This type of GSED can support pressures of 750 Pa. Large bore size enables a maximum field of view of approx. 1 mm in low vacuum mode, and the minimum attainable magnification is reduced by a factor of 2 to around 125× compared to a GSED with 0.5 mm bore size.

5.2.5 Gas Path Length

The average distance traveled by an electron without colliding with an air molecule is termed mean free path (MFP). The average number (n) of scattering events per electron depends on the total scattering cross section of the gas molecule for electrons (σ_g), the pressure of the gas (p_g), and the length of the path that an electron travels in gas (termed gas path length, GPL or simply L) and is given by:

$$n = \frac{\sigma_g \, p_g \, L}{kT} \qquad (5.1) \quad [23]$$

where k and T are the Boltzmann constant and the temperature, respectively. Under normal vacuum (10^{-3} MPa) at which the SEM operates, MFP is extremely large (several kilometers), and the electrons can travel the short distance through the column and the chamber without scattering. If gas pressure or the gas path length in the chamber is increased, the number of scattering events also increases. For instance, at 100 MPa (possible gas pressure used in low vacuum mode), the MFP

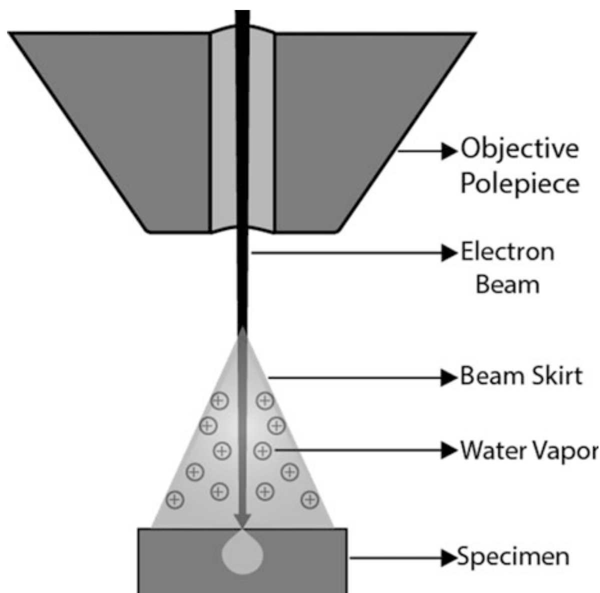

Fig. 5.7 Formation of beam skirt (electron beam scattering) due to the presence of water vapor above the specimen surface during imaging at low vacuum

reduces to around 10 mm. This is the typical working distance used in the SEM. Therefore, electron beam on its way to the specimen gets scattered at low vacuum. The scattered electrons move away from the focused beam and strike the specimen surface at a point away from the probe. This results in broadening of the electron beam which takes on a *skirtlike* form (Fig. 5.7). The skirt radius becomes large as the scattering increases and can be estimated with the following equation:

$$r_s = \frac{364}{E}\frac{Z}{}\left(\frac{p}{T}\right)^{1/2} L^{3/2} \qquad (5.2) \quad [23]$$

where r_s is skirt radius (m), Z is atomic number, E is beam energy (eV), p is gas pressure (Pa), T is temperature (K), and L is gas path length (m). This radius can be as large as 100 μm at an accelerating voltage of 10 kV, water vapor pressure of 10^3 Pa, and gas path length of 5 mm.

Schematics in Fig. 5.8a–c illustrate the electron beam scattering pattern with or without gas molecules present above the specimen surface. It can be seen in Fig. 5.8a that electron beam scattering in conventional SEM is rare and electrons travel straight to the specimen without any deflection. In the presence of high pressure and imaging gas inside the sample chamber, two cases are possible. The first case is shown in Fig. 5.8b where the beam will scatter, but the central part will remain in focus. This phenomenon is known as *oligo scattering*. The second case is illustrated in Fig. 5.8c wherein the presence of high pressure, the beam will scatter completely giving rise to *plural scattering*.

Figure 5.9a–c shows the beam intensity profile resulting from all three abovementioned cases, respectively. For the beam scattering cases shown in (a) and (b), there will not be much difference in the resolution of the image.

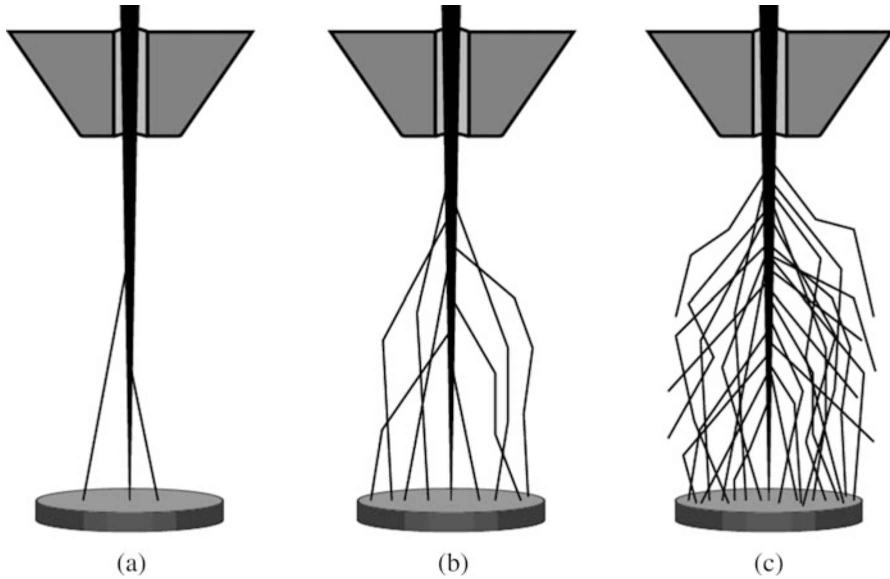

Fig. 5.8 Schematic showing scattering of the electron beam with increasing gas pressure from (**a**) to (**c**). An average number of collisions is defined as m in the figure. At $m = 0.05$, 95% of electrons do not have any collision [24]. (**a**) Minimal scattering; scatter < 5%; $m < 0.05$. (**b**) Partial scattering; 5–95% scatter; $0.05 \leq m \geq 3.0$. (**c**) Complete scattering; scatter > 95%; $m > 3.0$

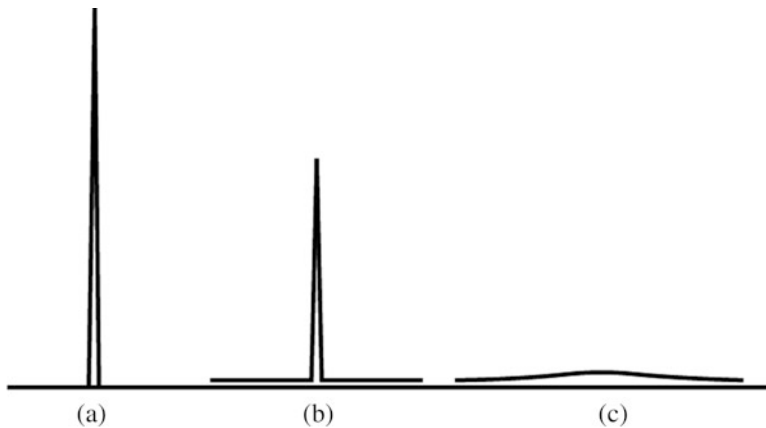

Fig. 5.9 (**a**–**c**) Schematics showing beam intensity profile corresponding to the three beam scattering cases shown in Fig. 5.8. (**a**) Minimal scattering regime; (**b**) Partial scattering regime; (**c**) Complete scattering regime

The skirt electrons result in the generation of a signal from the area of interest and its surroundings. However, a small amount of beam current is lost in the skirt, resulting in a lower signal from the point of beam impact. In case of (c), the beam is primarily scattered and a signal of appreciable strength is not generated.

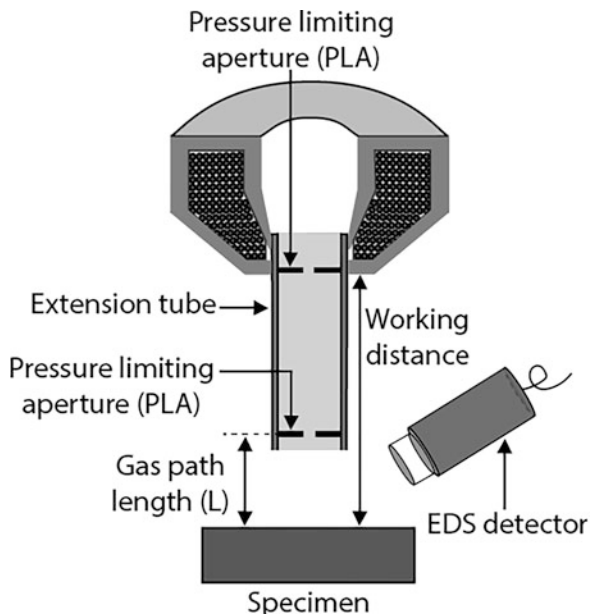

Fig. 5.10 Use of an extension tube mounted on the objective pole piece serves to reduce the gas path length (L) of electrons and results in less electron scattering in low vacuum mode

This scattering effect can be reduced by employing an extension tube with pressure-limiting aperture mounted at the end, as shown in Fig. 5.10. This long tube is fitted to the objective pole piece. Electrons enter this tube after emanating from the objective lens assembly. In this manner, the distance (gas path length) that the electrons have to travel in gas vapor is reduced, resulting in less scatter.

5.2.6 Applications

Types of specimens suitable for imaging using low vacuum capability include moist biological samples that shrink and change structure if dried. Likewise, insulating specimens such as polymers can also be imaged in a low vacuum without coating which occasionally tends to hide specimen features. Coatings may also interfere with microchemical analysis results. Similarly, wet colloids or oil-bearing rock samples can be examined in an as-received condition. Figure 5.11a, b show backscattered SEM images of a sample at high and low vacuum, respectively.

5.2.7 Latest Developments

Electron beam-gas interactions limit the imaging resolution of the microscope. However, improvements are being continuously made in this regard. At present,

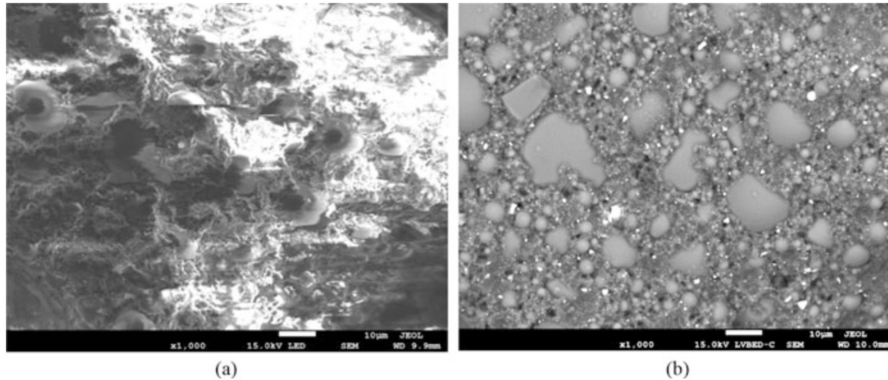

Fig. 5.11 Backscattered electron images of a sample at (**a**) high vacuum and at (**b**) low vacuum. Charge-up present at the specimen surface under high vacuum conditions is mitigated under low vacuum

field emission microscopes also offer low vacuum capabilities with improved spatial resolution. Pressure-limiting aperture is small (few hundred microns in diameter) allowing for greater pressure differences between the column and chamber. The vacuum in the chamber is easily controlled via a leak valve operated through computer software, and the type of gas used can be selected based on requirements. Since the PLA is placed close to the specimen, the distance the electron beam has to travel through the gas is shorter than the working distance employed during conventional microscopy.

5.3 Focused Ion Beam (FIB)

5.3.1 Introduction

The focused ion beam (FIB) is an instrument that uses positively charged heavy ions (instead of electrons) to raster the specimen surface. Use of ion source turns FIB into a versatile instrument. When the focused ion beam interacts with the surface of a material, it results in the generation of secondary ions, secondary electrons, and neutral atoms. Information from secondary electrons and secondary ions help in the formation of an image in the same manner as that in the SEM. The resolution of the FIB image can be as high as 5 nm.

Ions are heavier than electrons and carry a greater momentum. Use of heavy ions makes it easier to remove material from the specimen. Therefore, FIB is used for sputtering, etching, or micromachining of materials. It is also useful for milling, deposition, and ablation of materials. The FIB is used to modify or machine material surface on a micro- and nanoscale due to its ability to sputter materials with its positively charged heavy ions. Features that are milled can be as small as 10–15 nm in dimensions. One atom layer of a material can be etched without disrupting the

Table 5.1 Comparison between different characteristics of FIB and SEM sources

	FIB	SEM
Particle size	0.2 nm	0.00001 nm
Charge	+1	−1
Beam energy	Up to 30 keV	Up to 30 keV
Beam current	pA to nA	pA to μA
Penetration depth in Fe	20 nm (30 keV) 4 nm (2 keV)	1800 nm (2 keV) 25 nm (2 keV)
Generation of secondary electrons per 100 particles at 20 kV	100–200	50–75

layer underneath. Material removal and deposition can be controlled to a nanometer scale. Different gases can be injected into the system near the surface of the specimen to deposit required materials.

Imaging capability enables it to carry out these operations on specific sites selected by the user. It can be used to characterize and fabricate semiconductor materials and also prepare thin film sections for examination in a transmission electron microscope. Since ions are positive, large, and heavier compared to electrons and react only with outer shell electrons of the specimens, they exhibit high interaction probability and low penetration depth in specimens. Ions can also be used as dopants since they can be trapped easily due to their large mass. Comparison of ions and electron characteristics is given in Table 5.1. The spatial resolution of images generated using SEM is greater than those of the FIB. Focused ion beam uses a column similar to the one used for the SEM. It is widely used in semiconductor industry for failure analysis, circuit writing, thin sample preparation, etc.

A schematic of FIB system is shown in Fig. 5.12.

High current density removes the atoms or molecules from the surface of the specimen called sputtering. Using high current density, micromachining or milling is also achieved as the ions carry a large amount of energy and momentum. Small current density does not sputter a greater amount of material, but it still generates secondary electrons which are then used to get an image as in the SEM.

An advantage of focused ion beam over scanning electron is the characterization of a nonconducting sample which can be imaged using positive primary ion beam. An electron flood gun with low energy is used to neutralize the charge on the surface of the specimen generated by the focused ion beam, and the positive secondary ions are collected by the detector to get an image without destroying the specimen. The FIB is also equipped with gas injectors to produce specific chemical reactions at the surface during ion beam-assisted deposition or etching process. Due to adequate resolution attained in modern FIB instruments, use of a separate SEM may not be required for imaging. However, instruments are available that are equipped with two columns, one for FIB and the other for SEM (see Fig. 5.13). In these instruments, specimens can be prepared with FIB and can be examined using high-resolution SEM. Thin transparent TEM foil is prepared using FIB column and is imaged using STEM detector located within the same combined equipment. Availability of such

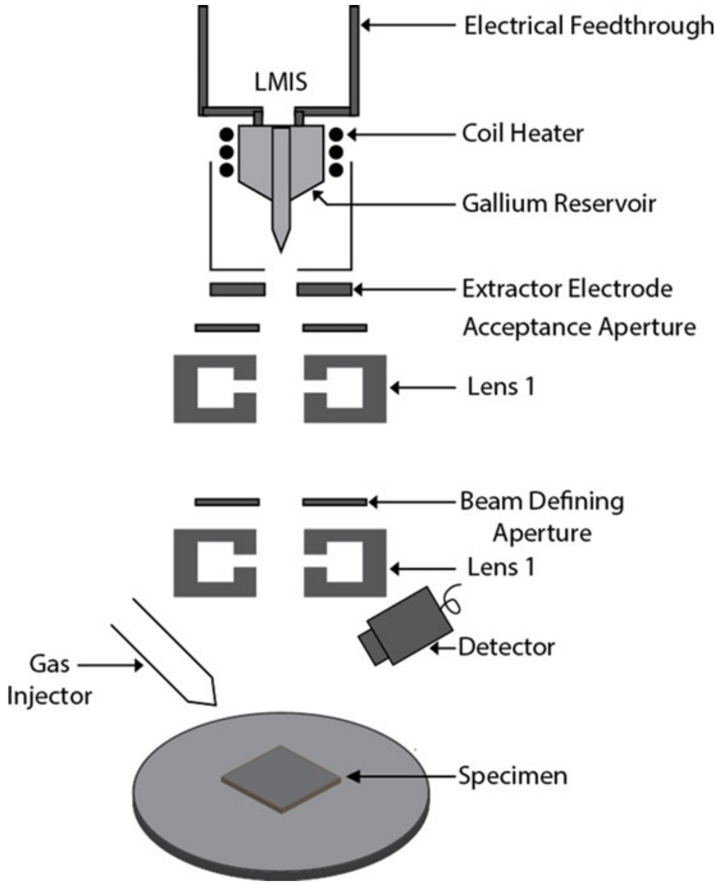

Fig. 5.12 Schematic showing various components of FIB

equipment has made it possible to undertake high-resolution 3-D microscopy and nano-tomography.

The FIB has become a popular instrument for materials science and semiconductor industry applications. It is used for defect analysis, circuit board preparation, and repair in the semiconductor industry. It is widely used to prepare cross-sectional TEM samples in research labs. Specimens with thin areas at specific locations such as grain boundaries, cracks, pits, etc. can be produced. The ability of FIB can be seen in the example shown in Fig. 5.14 where word "KFUPM" has been milled on an aluminum alloy surface.

Focused ion beam is widely used for TEM sample preparation. The steps involved in such a preparation are shown in Fig. 5.15.

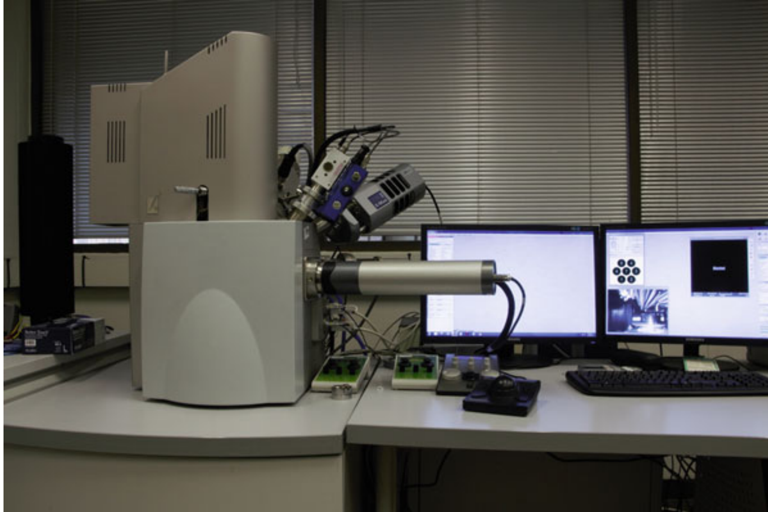

Fig. 5.13 FIB-SEM combined instrument with two columns; the vertical column is for the SEM, and the inclined column (hidden under enclosure) is for FIB

Fig. 5.14 The word "KFUPM" is milled onto the surface of Al alloy using focused ion beam

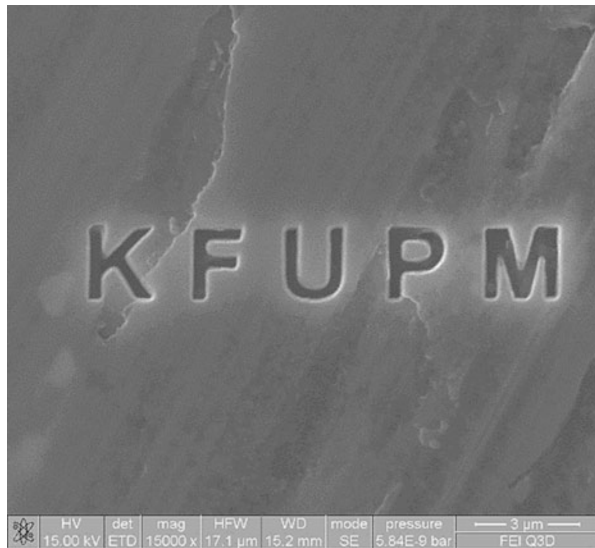

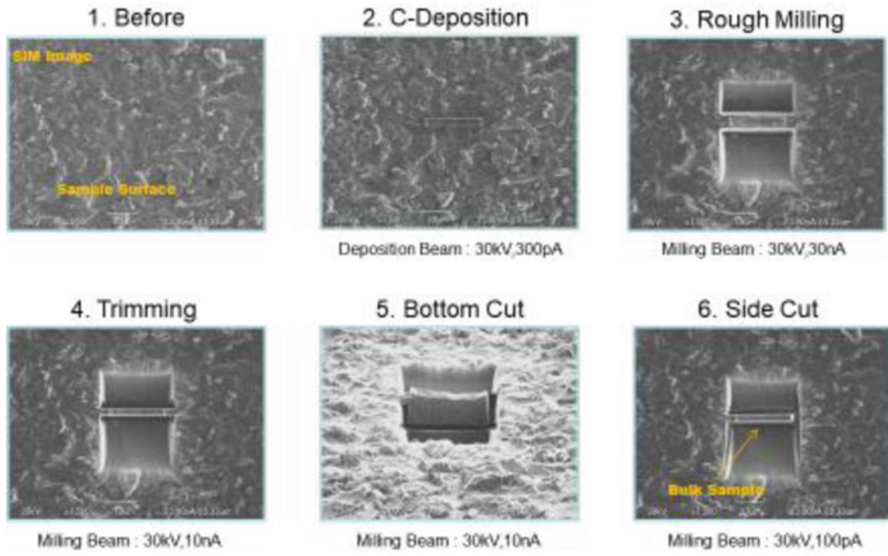

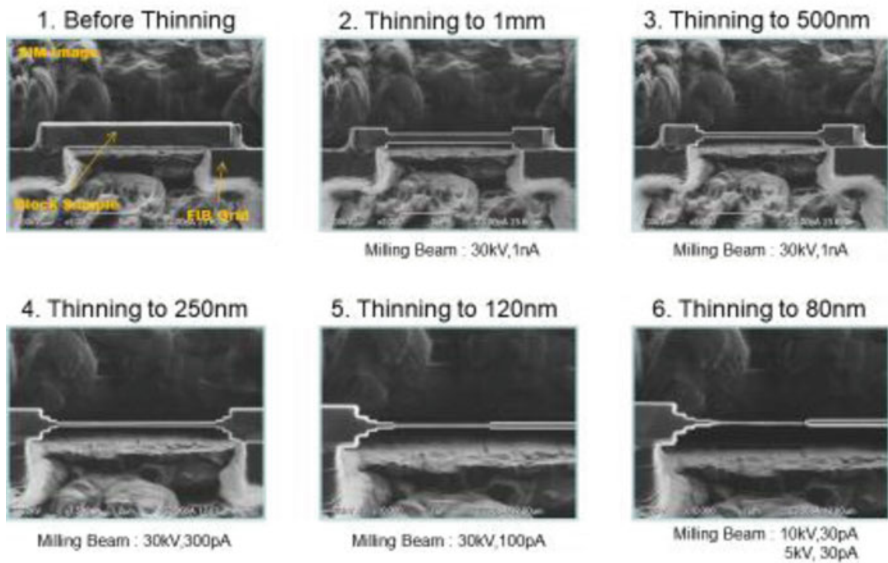

Fig. 5.15 Thin foil (lamella) sample preparation for transmission electron microscope (TEM) using a focused ion beam instrument. Complex cross-sectional samples can be made within hours. At high beam currents, a large amount of material is removed which allows very fast site-specific milling of specimens compared to that done using argon ion milling

5.3.2 Instrumentation

Focused ion beam equipment consists of a column, specimen chamber, vacuum system, detectors, gas input system, and a computer-controlled system. The column contains ion source, electrostatic lenses, beam acceptance and beam-defining apertures, blanking plates, a steering quadrupole, an octupole deflector, and detectors.

5.3.2.1 Ion Sources

There are three types of ion sources that can be used in FIB, namely, (a) liquid metal ion source (LMIS), (b) gas field ion source, and (c) volume plasma source.

(a) *Liquid Metal Ion Source (LMIS)*

The most commonly used ion source in FIB technique is liquid metal ion source with gallium as source metal. Gallium has a low melting point, low volatility, low vapor pressure, high stability, long service lifetimes, and excellent electrical, mechanical, and vacuum properties. It exhibits good emission characteristics that enable high angular intensity with a small energy spread. It shows no overlaps with other elements in the EDS spectrum. Other metals like Cs, Au, Pb, Bi, etc. can also be used depending on the requirement. Ions are generated from the metal by electrospray technique where tungsten needle and gallium metal are placed in contact with each other (see Fig. 5.16). The liquid gallium is heated and directed to the tip of the needle and stays there due to surface tension. A voltage is applied to create an electric field which results in

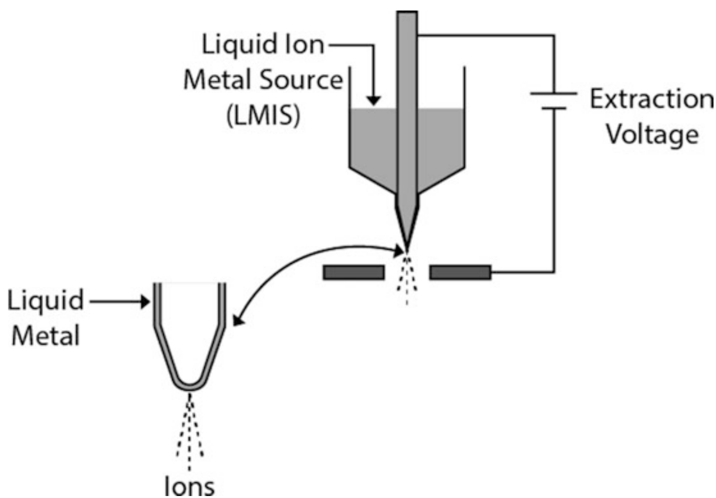

Fig. 5.16 Liquid metal ion source used in the FIB technique to generate ions. Schematic shows the formation of ions at the Taylor cone tip and their movement toward the electrostatic lenses [25]

Taylor cone formation which is the shape the liquid metal takes at the tip of the tungsten needle. The radius of the cone tip is about 2 nm. When the voltage is further increased, it results in the ejection of liquid metal from the cone tip in a thin stream. This technique is known as *electrospray* technique. The electric field acting on the cone tip is more than 1×10^8 V/cm that ionizes the liquid metal, and field ejects the ions. Ions are accelerated to 1–50 kV toward the electrostatic lens. This method produces high current density focused ion beam which has a very small spot size in the range of a few nanometers.

(b) *Gas Field Ion Source (GFIS)*

The setup of gas field ion source is similar to the liquid metal ion source. The only difference is that the liquid metal is replaced with a condensed gas. Usually, noble gases are used. Most common gases used are H_2, He, Ar, N, etc. The tungsten needle is kept at cryogenic temperatures. The gas is inserted and condensed at the needle tip. The cryogenic temperature of the needle helps in the condensation of the gas. Then an electric voltage is applied across the needle and the other electrode which results in the ionization of the gas in the same manner as in the liquid metal ion source. The current density can be enhanced by increasing the electric field at the protrusion of condensed gas. The smaller the size of the condensed gas cone tip, the greater will be the electric field and hence the higher the current density. By making the size of cone tip smaller, the electric field lines can be forced to get almost parallel to each other resulting in a very focused and thin ion beam which increases the brightness of the image [25]. Due to the short service lifetimes of around 160 h, this source has not found commercial use.

(c) *Volume Plasma Sources (VPS)*

Volume plasma sources are used for metal deposition, lithography, and ion milling machines. The desired species to be implanted is introduced in the form of gas and is bombarded with electrons to create the plasma, and an electric field is applied to accelerate the ions toward the substrate. Volume plasma ion sources generate a high current density although the ions are not emitted from a single point as in LMIS and GFIS. A brief comparison of ion sources is included in Table 5.2.

Table 5.2 Comparison of different ion sources [25]

Ion source	Ion species	Virtual source size (nm)	Energy spread (eV)	Brightness (A/cm^2 sr)	Angular brightness (μA/sr)
Liquid metal	Ga^+	50	>4	3×10^6	50
Gas field	H^+, H^{2+}, He^+	0.5	~1	5×10^9	35

5.3.2.2 Lens System

Unlike scanning electron microscope, focused ion beam instrument uses electrostatic lenses which focus the ions near to the lens. Upon generation, ions are accelerated in the form of a beam under the influence of an applied voltage toward the beam acceptance aperture and enter the condenser lens. Steering quadrupole of the condenser lens aligns the beam so it can pass through the center of the beam defining aperture. Steering quadrupole of the objective lens adjusts the trajectory of the beam with the optical axis of the objective lens. The blanking apertures present between the condenser and the objective lenses protect against constant milling of the specimen by the ion beam. The octupole deflectors present below the objective lens provide astigmatic correction.

5.3.2.3 Stage

The stage is fitted in the specimen chamber and holds the sample while it is being bombarded with the ion beam. One can maneuver the stage in X and Y axes either by rotation or by traversing. The stage can also be tilted as per requirement.

5.3.2.4 Detector

The detector consists of a glass array having millions of tiny channel electron multipliers forming a microchannel plate (MCP). Charge species formed after ion beam interaction with the specimen are attracted to the detector resulting in the formation of an image or in the identification of elements. Scintillators are also part of the detection system which are made from a material that converts electrons or other radiations into a photon. Detectors are just mounted at some angle above the specimen to get secondary particles generated from ion-solid interactions.

5.3.3 Ion-Solid Interactions

When a primary ion strikes the target material or solid specimen, it transfers its energy and momentum to the solid, and a number of phenomena take place, including sputtering, backscattering, ion reflection, electron emission, electromagnetic radiation emission, specimen damage, ion emission etc. The primary ion after losing all its energy comes to rest and gets deposited in the solid. During this period, from striking until deposition, it strikes a number of atoms resulting in a collision cascade. Since the primary ion carries energy and momentum, two types of ion-solid interactions can take place: elastic interactions and inelastic interactions. During the inelastic interaction, striking of a primary ion with the specimen ionizes some of the neutral atoms in it resulting in the generation of some electromagnetic radiation and emission of electrons, whereas during elastic interaction between primary ions and the specimen, primary ions transfer their energy to the specimen atoms or molecules in the form of translational energy resulting in the knocking out of atoms from the specimen or causing displacement from the initial position. This leads to damage of the specimen. The probability of inelastic scattering between a specimen and electron beam is less as compared to that of between a specimen and ions.

The energy needed to displace an atom from its original site is known as displacement energy. It is a critical value of energy. When a high-energy ion strikes a solid, it may transfer its energy as translational energy to a solid atom. If this translational energy is greater than the critical displacement energy, the ion will knock out the solid atom from its site generating a defect known as an interstitial-vacancy point defect. The primary high-energy ion may have some energy left after this collision. If this is the case, the primary ion will still move forward striking more solid atoms in its path displacing them from their original site and resulting in a cascade of collisions until it loses all its energy and gets embedded in the solid. If the interaction only happens near the surface of the solid, the recoiling atom has a chance to get out of the solid after the collision, leading to sputtering. Here it should be understood that the displacement energy is always higher than the binding energy between the two atoms which indicates that the collisions are nonadiabatic. After the primary ion has stopped, the result is the emission of electromagnetic radiation, some particles (electrons, ions, etc.), lattice defects, heat and incorporated primary ion in the solid. Monte Carlo calculations are suitable for simulation of collision cascade due to ion-solid interaction. In inelastic collisions, most of the energy of the primary ion is lost due to solid heating or vibrations of solid atoms rather than displacement.

5.3.4 Ion Imaging

Ion beam scans the surface of the specimen like the electron beam in scanning electron microscope resulting in the generation of electrons, ions, and electromagnetic radiations. In case of scanning electron microscope, the resulting electrons are called secondary electrons which are generated when electron beam hits the sample. In focused ion beam microscopy technique, the resulting electrons are often known as ion-induced secondary electrons and have low energies. For each 5–30 keV Ga ion hitting the surface of the sample, around ten ion-induced secondary electrons with an energy of 10 eV each are generated. The surface of the sample may have been oxidized before the ion beam strikes it; therefore, the electron yield ejecting out of the sample might be low. But as the ion beam strikes the surface, it results in the sputtering of the oxidized layer, resulting in the removal of a large number of electrons. Thus electron yield changes with time and is more when the surface is clean.

Electron beams are more focused than ion beams; therefore, the resolution due to the ion beam is lesser than that of the electron beam. But the focused ion beam provides a greater channeling contrast as compared to that provided by the SEM. When crystal orientation is such that the primary ion channels through the atoms in the sample, there are fewer interactions of a primary ion with the atoms, and the induced secondary ion yield is less. But when the orientation is such that primary ion channels through the atoms but interacts with more atoms near the surface, more induced secondary electrons escape from the surface of the sample resulting in a higher contrast. Atomic mass has a direct relationship with the contrast of the image. The heavier the atomic mass of the sample, the greater is the probability of

generation of secondary induced electrons as compared to that of the sample with lower atomic weight. Surface geometry also affects the contrast of the image.

5.4 STEM-in-SEM

Traditionally, transmission electron microscopes (TEM) have been used to study the microstructure of materials at high accelerating voltages of 120–300 kV. In this type of microscope, the electron beam is transmitted through the specimen to form an image. The TEM can be equipped with a scanning mode where the beam is scanned and transmitted through the specimen at the same time. This type of equipment is known as scanning transmission electron microscopes (STEM). In another variation, a specialized TEM that can only be used in the scanning transmission mode is called "dedicated" STEM. However, advances in technology have enabled the use of SEM in a scanning transmission mode, providing a cost-effective alternative. This is undertaken by mounting a STEM detector within the SEM and using ultrathin specimens that are transparent to electrons at 30 kV. Resulting STEM-in-SEM is used to undertake scanning transmission electron microscopy in addition to the conventional study of the surface topography of materials. STEM detector is considered an important tool that serves to enhance the characterization capability of the SEM without having to invest heavily in the acquisition of the more expensive transmission electron microscope. Use of STEM detector allows imaging of inner structural details of materials such as alloys, coatings, carbon nanotubes, nanopowders, catalysts, etc.

5.4.1 Working Principle

Scanning transmission electron microscope (STEM) detector is mounted below the sample stage and is used to collect electron signal transmitted through the specimen. The stage is altered to allow the continued progression of the electron beam and also to create space for the placement of STEM detector. The specimen has to be thin enough to transmit an electron beam with an accelerating voltage typically used in the SEM. A small probe is scanned across the sample surface, and the detector collects the signal after the beam is scattered and transmitted through the specimen. Image formation is similar to a conventional SEM where signal obtained from a specific location of the specimen during the scan is processed through the detector and displayed on a corresponding location on a monitor that is scanned in sync with the beam scan. The strength of signal obtained from a pixel of the specimen determines the intensity of the corresponding pixel on the monitor during the synchronized scan. Fine powders and nanotubes can be examined in an as-received condition, while metallic specimens are prepared using standard TEM sample preparation techniques such as electro-jet polishing and ion beam milling.

A STEM detector can be a scintillator/photomultiplier or solid-state type detector as shown in Fig. 5.17a. This type of detector is used to form both bright and annular

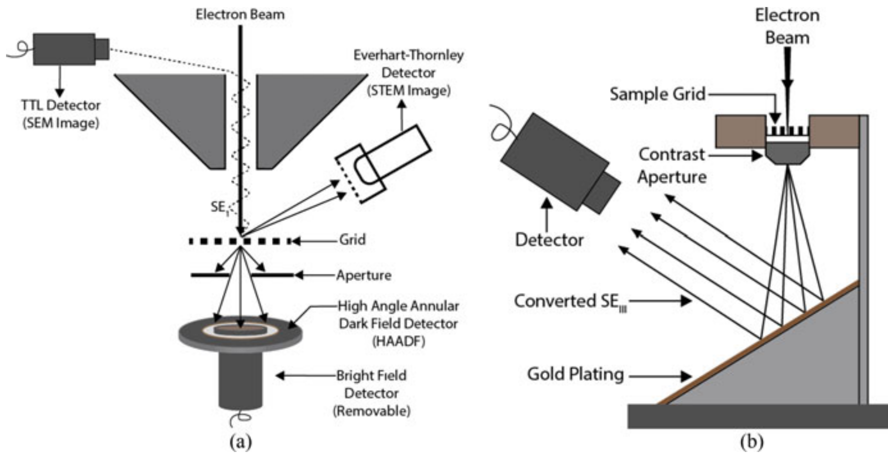

Fig. 5.17 (**a**) Schematic representation of STEM-in-SEM arrangement where the electron beam is scanned over and transmitted through an ultrathin specimen. Electrons scattered at low angles are collected by a bright field (BF) detector, and those scattered at high angles are intercepted by high-angle annular dark field (HAADF) detector. (**b**) Schematic representation of less expensive "STEM converter" arrangement where the beam transmitted through the specimen is scattered by slanting Au-coated Si surface. Secondary electrons generated due to beam interaction are collected by a conventional E-T detector placed in the specimen chamber

dark field images. The bright field image is formed by collecting electrons that are scattered at small angles and are centered on the optic axis of the microscope while passing through the specimen (e.g., *direct beam*). The *incoherent* dark field image is formed by (off-axis) electrons scattered at high angles and shows the atomic number and mass-thickness contrast. The degree of contrast shown by different elements varies depending on their atomic number. The detector that collects the strongly scattered electrons to form a high STEM image contrast is called high-angle annular dark field (HAADF) detector. The size of the detector is fixed, but the collection angle of the detector can be varied by moving the detector away or close to the specimen. Use of a multi-segment detector allows collection of signals by each segment independent of each other which then can be added or subtracted to form an image.

An inexpensive alternative to the scintillator or SSD device is to have a "STEM converter" as shown in Fig. 5.17b. In this arrangement, the beam transmitted through the specimen passes through an underlying small aperture (few mm in diameter) and is scattered by Au-coated mirror surface placed at an angle. The impact generates secondary electrons that are collected by a conventional E-T detector available in the specimen chamber. Aperture size can be changed to vary contrast. Smaller-sized aperture will produce stronger contrast but a smaller field of view. This type of detector is less expensive but forms images with low signal-to-noise ratio and is used for bright field imaging only. Through-the-lens (TTL) detector placed in the column above the specimen can be used to capture the signal scattered upward.

The STEM detector is usually installed in a high-end microscope equipped with a field emission gun to take advantage of its high brightness. Employment of immersion or snorkel objective lens allows the use of short working distance which reduces spherical aberration in the lens and creates a fine probe. Additionally, use of thin section restricts the size of interaction volume within the specimen resulting in an enhanced spatial resolution of 0.6 nm in the STEM-in-SEM [3]. Since the specimens are electron transparent, the contrast formed is similar to that in a conventional TEM.

5.4.2 Advantages/Drawbacks

Ability to observe multiple specimens, automated stage navigation, efficient analysis, ease of use, and cost-effectiveness along with enhanced resolution and contrast have made this technique popular with life and materials scientists working with biological and polymeric thin sections and nanopowders. Use of low accelerating voltage (typically 30 kV) in STEM-in-SEM reduces the probability of beam damage and provides enhanced contrast for the low atomic number and low-density materials. Bright field and dark field images can be recorded simultaneously during a single scan. Owing to a lack of imaging lens below the specimen, the solid angle of collection of transmitted electrons is large resulting in substantial signal-to-noise ratio. Owing to thin electron-transparent samples, signals originating from depths of the sample are eliminated. The transmitted electrons carry information about the internal structure of the material under examination. However, low electron beam energy used in this technique requires the specimen to be adequately thin to be electron transparent. Due to a different configuration than standard STEM equipment, image interpretation can be relatively complicated.

5.4.3 Applications

Imaging of submicron sized or nanopowders presents a challenge in the conventional SEM, especially if the powder material is composed of light elements. Electron beam penetrates the fine powder grains and is scattered. The volume of scattering produced within the material, known as the interaction volume, is bigger than the grain size of the powder itself. Consequently, the beam is scattered off the substrate material that is used to hold the powder specimen. Electrons scattered from the substrate contribute to the noise in the signal and diminish the image quality. In nano-sized particles, the noise dominates the signal, and contrast from the powder becomes too low to resolve its features. Use of a STEM detector can overcome this problem. The fine powder is placed over a copper grid coated with a holey carbon film (3 mm diameter, routinely used for examining TEM specimens) to reduce scattering from the substrate. The electron beam is transmitted through the powder specimen and collected by the STEM detector to form an image as shown in Fig. 5.18.

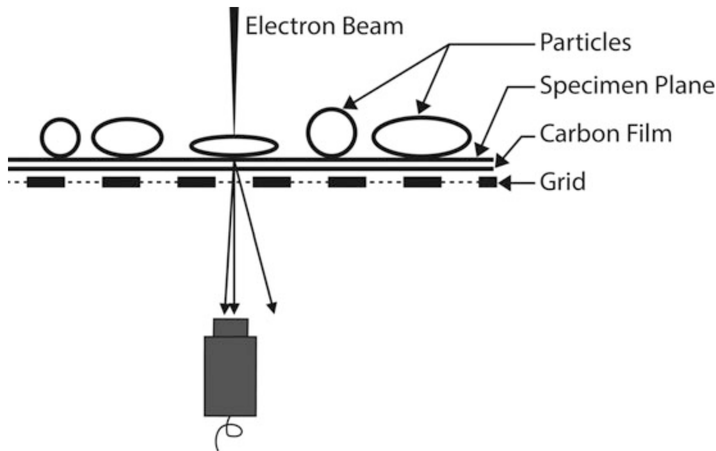

Fig. 5.18 Schematic representation of imaging of nanopowders in STEM-in-SEM. The specimen is placed over a thin carbon film to reduce extraneous scattering from the specimen holder. Use of thin holder reduces noise in the signal

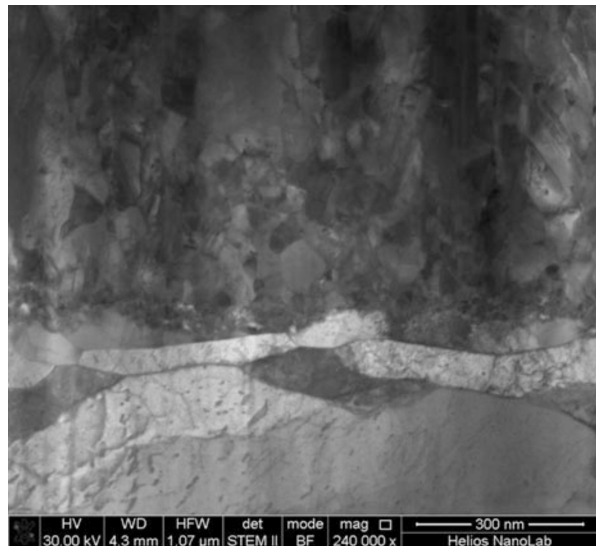

Fig. 5.19 High-angle annular dark field (HAADF) STEM image showing Ni coating on steel substrate in cross-sectional view. Grain boundaries, coating-substrate interface, and dislocations present in the substrate underneath the interface are clearly visible in one plane

Thin specimens for STEM imaging are prepared using electropolishing, argon ion milling, or focused gallium ion beam methods. Due to the thinness of the specimen, the transmitted image lacks contribution from low-resolution backscattered or SE_2 signals, thereby resulting in improved resolution and image contrast. Normally, STEM microscopy is conducted with the highest accelerating voltage available in the microscope to enable maximum transmission and brightness in the image. An example of a bright field STEM image of a cross-sectional specimen of Ni deposited on steel substrate is shown in Fig. 5.19. The image clearly shows grains of Ni along

with its grain boundaries, coating-substrate interface, and dislocations present in the substrate underneath the interface.

5.5 Electron Backscatter Diffraction (EBSD)

Usually, phases in a material are identified in the SEM using microchemical analysis with EDS technique. This kind of analysis cannot be termed conclusive. For instance, TiO_2 may have different crystal structures with the same composition. Other phases such as iron oxides may exist as FeO, Fe_2O_3, or Fe_3O_4, and it may not be possible to distinguish them solely on chemistry. Another example is the identification of austenite and ferrite in steels which is not possible using EDS due to low carbon contents. This limitation in the SEM can be overcome by electron backscatter diffraction (EBSD) technique which can determine crystal structure as well as grain orientation (texture) of materials. Material surface is specially prepared for this analysis, and specimen is tilted at approx. 70° from the normal position. High accelerating voltage such as 20 kV is used to strike the specimen surface resulting diffraction of backscattered electrons from the specimen planes that are imaged as straight lines. Different orientation of planes at a specimen surface produces various sets of intersecting straight lines called Kikuchi pattern. The relationship between these lines determines the correlation between atomic planes. For instance, the distance between lines represents angles between crystals. Indexing of Kikuchi patterns is done using dedicated software which is used to calculate structural information and measure grain orientation. Specialized equipment such as EBSD detector with a phosphor screen and CCD camera, as well as computer software to control acquisition and processing of EBSD data, are required to undertake such an analysis. EBSD detectors in the modern field emission SEMs are able to examine materials with fine grains down to 100 nm in dimensions.

Availability of EBSD in SEM greatly enhances the latter's power as an analytical tool. With this addition, the SEM can not only be used to examine surface morphology and determine chemistry but also obtain crystallographic information from the material. Ability to determine crystal structure greatly improves the ability to identify unknown phases. Crystallographic information that can be gathered using this technique includes crystal spacing, crystal symmetry, and the angle between planes. Low- and high-angle boundaries between crystals can be determined by calculating the angles between grains. This technique has found application in the study of recrystallization and grain growth. EBSD can acquire crystallographic data from a crystalline specimen and correlate it to its microstructure. It is used to identify phases and study phase fractions/distribution, grain size/shape, aspect ratios, strain, material texture, crystal symmetry/orientation, defects, and grain boundaries. Traditionally, such type of structural analysis had been conducted using transmission electron microscopy.

5.5.1 Brief History

The exploration of diffraction which lays the foundation of present-day EBSD can be linked back to the year 1928 when an electron beam with an energy of 50 keV, and an angle of incidence of 6° produced from a gas discharge was directed on to a cleavage face of calcite by Seishi Kikuchi [26]. The patterns which emanated as a result of diffraction were captured onto photographic plates positioned 6.4 cm in front and back of the crystal. The patterns were described as "…black and white lines in pairs due to multiple scattering and selective reflection."

Nine years later, in 1937, the same phenomenon was observed by Boersch [27], and he was able to produce some excellent patterns on photographic film. Both transmission and backscattered diffraction patterns from cleaved and polished surfaces of various materials including NaCl, KCl, quartz, mica, diamond, Cu, and Fe were reported by him. In 1954, Alam, Blackman, and Pashley [28] used a cylindrical specimen chamber and a film camera to produce high-angle diffraction patterns from cleaved LiF, KI, NaCl, and PbS_2 crystals.

The coming of commercial SEM in 1965 paved the way for marked progress during the years from 1969 to 1979 where three prominent discoveries came to light. These included selected area channeling patterns (SACP) by Joy et al. at Oxford [29], Kossel diffraction by Biggin and Dingley at Bristol [30], and electron backscatter patterns (EBSP) by Venables and Harland at Sussex [31]. A TV camera and a phosphorous screen were employed for the first time to record the EBSP patterns.

5.5.2 Working Principle

In a crystalline specimen, atoms are positioned in a regular periodic three-dimensional arrangement called lattice. In this technique, electrons from the primary beam (10–30 kV accelerating voltage, 1–50 nA incident current) in an SEM strike the surface of a tilted (70°) and highly polished flat strain-free crystalline specimen and are scattered forming an interaction volume within the specimen. Backscattered electrons spread in all directions within the interaction volume. This can be thought of as a divergent source of electrons present within the specimen close to the surface. Part of these high-energy backscattered electrons is incident on sets of parallel lattice planes present within the crystal and are scattered in a manner that satisfies Bragg's equation which is written as:

$$n\lambda = 2d\sin\theta \quad (5.3)$$

where n is the order of diffraction, λ is the electron wavelength, d is the lattice plane spacing, and θ is the Bragg angle of diffraction. This type of scattering is termed as electron diffraction. This is constructive interference of electron waves where the difference in path length traveled within a single lattice plane between two waves is a multiple of λ and the incident and emergent angles of the wave are equal. Upon scattering within the specimen, the electrons spread in all directions, and for each set

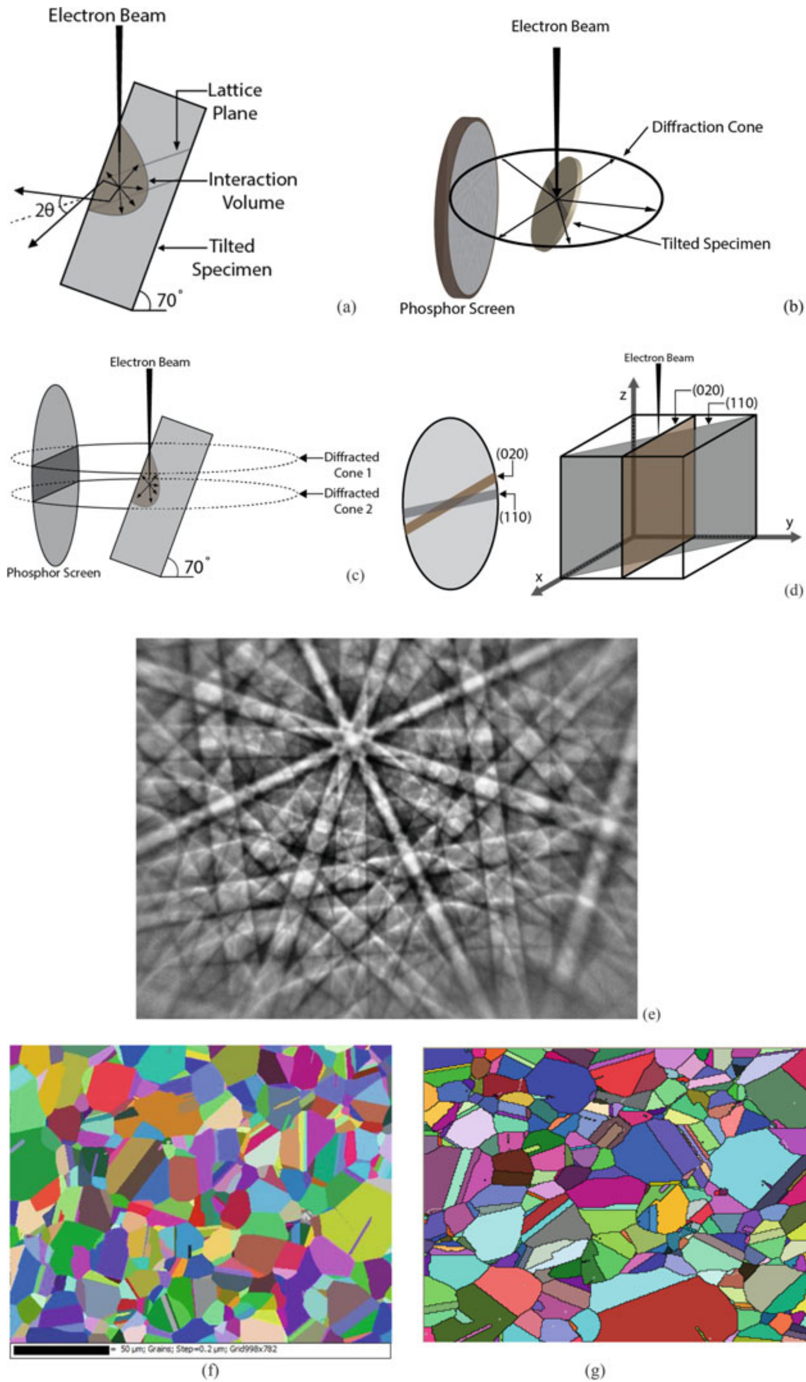

Fig. 5.20 (**a**, **b**) Electron scattering acts as a divergent source of electrons within a specimen. These electrons are incident upon a lattice plane satisfying Bragg's equation. Resulting diffraction forms a pair of cones at the front and back end of the plane. (**c**) Diffracted rays are formed along the

of lattice planes for which the above Bragg condition is fulfilled, the diffracted beams emerge out of the specimen in all directions in the form of a cone (see Fig. 5.20a, b). Diffracted beams lie on the surface of this cone whose axis is normal to the diffracting lattice plane. In fact, two cones are formed for each set of lattice planes, one at the front and the second at the rear of the lattice plane, as seen in Fig. 5.20c. These cones intersect the phosphor screen as two dark lines bordering a bright band. Bragg reflections emanating from various planes present within a specimen give rise to a network of a pair of sharp lines with bright bands intersecting each other at various angles. This network is called Kikuchi pattern and consists of a set of parallel lines crossing each other at different angles. Every set of two parallel lines represent a family of parallel planes with a specific value of *d*-spacing. One line represents the positive and the other line represents the negative plane, and the distance between the two lines is inversely proportional to the *d*-spacing for that specific plane.

Kikuchi pattern can be used to determine crystal orientation, angles between lattice planes, bend contours, electron channeling patterns, and fringe visibility maps. Projection of lattice planes in a Kikuchi map is shown schematically in Fig. 5.20d. A typical Kikuchi pattern is shown in Fig. 5.20e. The width of a Kikuchi band is determined by Bragg conditions and the distance between the specimen and the phosphor screen. The surface area of a specimen can be scanned to obtain an EBSD map from each scanned point in that area (see Fig. 5.20e). EBSD grain maps of stainless steel and Al are shown in Fig. 5.20f, g, respectively.

5.5.3 Experimental Setup

The experimental setup used for EBSD in an SEM is shown in Fig. 5.21a. The specimen is tilted to 70° using a pre-tilt holder or the SEM stage. At high tilt angles, near-surface material is excited, and the total interaction volume formed close to the surface is very large compared to the interaction volume deep within the material. Formation of large interaction volume close to the specimen surface allows easy escape of electrons from within the specimen and thus increases the ratio of diffraction component to the yield of backscattered electrons. Without the use of high tilt, the proportion of diffracted electrons in the overall electron yield may be too low to be detected, and adequate contrast may not be produced in the pattern. The detector for EBSD is attached to one of the free ports in the specimen chamber. Its front end consists of a fluorescent phosphor screen as shown in Fig. 5.21a. The screen converts electrons emanating from diffracting planes of the specimen into light which passes through a lead glass window located after the phosphor screen. Lead glass serves to isolate the detector assembly from the evacuated SEM chamber

Fig. 5.20 (continued) surface of cones and strike the phosphor screen resulting in a pair of lines for each set of lattice planes. (**d**) Schematic illustration of electron beam interaction with the lattice planes giving rise to Kikuchi bands on a phosphor screen (**e**) Kikuchi pattern obtained from a bcc iron. EBSD grain map of (**f**) stainless steel and (**g**) Al

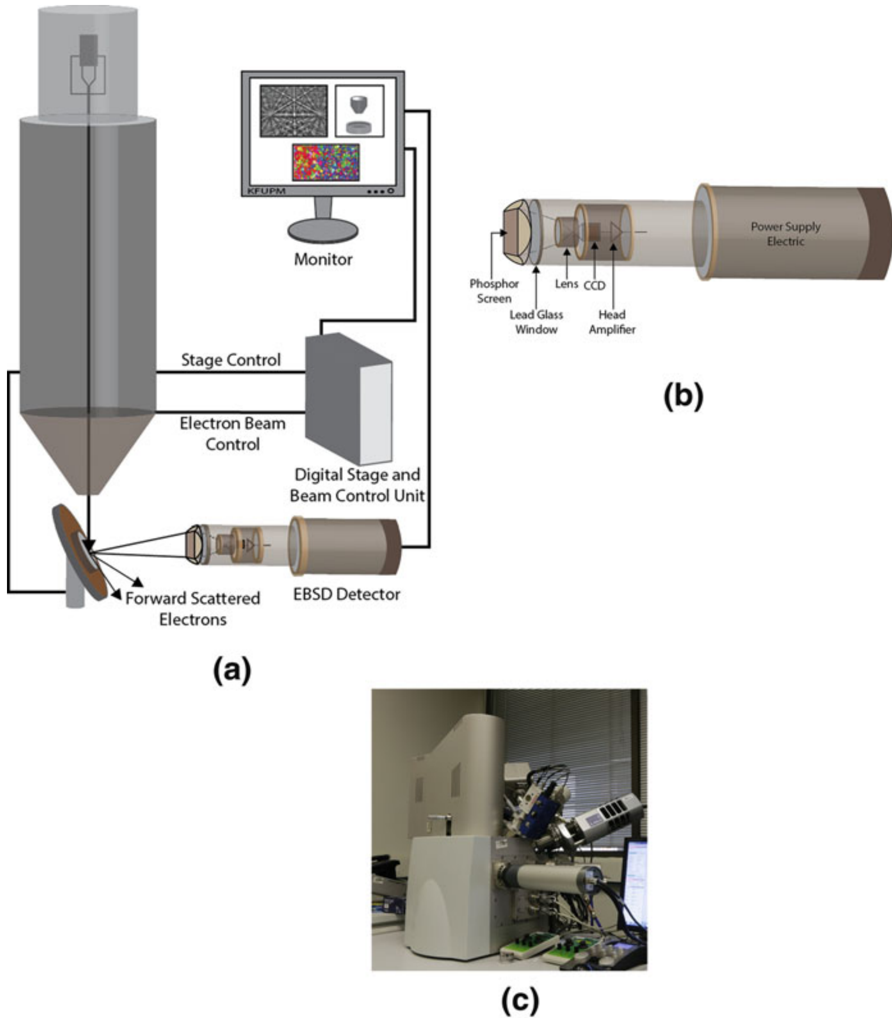

Fig. 5.21 (**a**) Standard experimental setup for electron backscatter diffraction (EBSD) in SEM showing a crystalline specimen tilted 70° toward the phosphor screen. The diffracted pattern generated due to specimen-beam interaction intersects the screen that converts electrons into light which is then imaged using a CCD camera. The Kikuchi patterns and mapped images are displayed onto the computer screen. Forward scattered electrons can be detected by placing an optional diode detector at the lower end of the EBSD detector. (**b**) Illustration of an EBSD detector which includes a phosphor screen, lead glass window, lens, CCD camera, amplifier, and associated electronics in a single compact assembly. (**c**) An EBSD detector is seen fixed to the specimen chamber of an SEM

while allowing light to pass through it. The light travels through a lens and onto the surface of a sensitive CCD camera which detects it and converts it into an image. The pattern formed on the phosphor screen is visualized and imaged with the help of this camera. The signal is then amplified and fed to the computer for display onto the

monitor. Schematic and photograph of a compact design EBSD detector are shown in Fig. 5.21b, c, respectively. Diffracted electrons form only a small proportion of the total number of electrons scattered from within the specimen that strikes the phosphor screen. In other words, Kikuchi pattern is superimposed on a background which needs to be removed to make visualization possible. Materials with a high average atomic number (i.e., with high electron scattering factors) produce a relatively larger number of diffracted electrons resulting in higher contrast in the electron backscatter patterns (EBSP).

Electron backscatter diffraction detector is usually coupled with a Schottky field-emission electron microscope which provides high stable beam current and good mechanical stability. These characteristics are important since the acquisition of high-resolution large orientation EBSD maps can take several hours. EBSD is an extremely surface-sensitive technique with information acquired from depths of only a few to tens of nanometers. Surfaces are generally prepared using electropolishing or ion milling to remove any deformation.

5.5.4 Applications

Types of materials examined with EBSD include metals, alloys, minerals, ceramics, thin films, solar cells, intermetallics, and semiconductors. EBSD is used to identify and determine the distribution of intermetallic phases, secondary phase particles, precipitates, and minerals in a wide variety of materials. Each EBSD pattern is unique, and its characteristics are governed by lattice parameters of the crystal under examination, positioning of that specific crystal in 3-D space, the wavelength of the incident electron beam (which is proportional to the acceleration voltage), and the distance between the sample to the EBSD detector. Angles between bands within a Kikuchi pattern are measured to distinguish between different crystal structures with varying unit cell dimensions and interplanar angles. Phases that possess the same crystal structure but different lattice parameters can be differentiated by using more complicated routines that also measure bandwidth in Kikuchi patterns.

Dedicated software programs are used to index the Kikuchi patterns and display EBSD maps. One method of indexing is to provide crystal structure information and microscope operating conditions to the computer. The computer program measures the position of the Kikuchi lines and calculates the angles between them to compare the data to the provided crystal structure. In this manner, the crystallographic orientation of the specimen is determined. In another method, EBSD patterns obtained from various points are indexed by the software program and compared to the stored values of crystallographic lattice planes in the database (i.e., crystallographic indices of lattice planes, lattice spacing d, the interplanar angles, and intensity of lattice planes) to report the best fit for identified phase and its orientation. Kinematical electron diffraction model is used to determine the best fit. Study of grain size, orientation, and morphology is another common application of EBSD. Distribution of high- and low-angle grain boundaries and twin

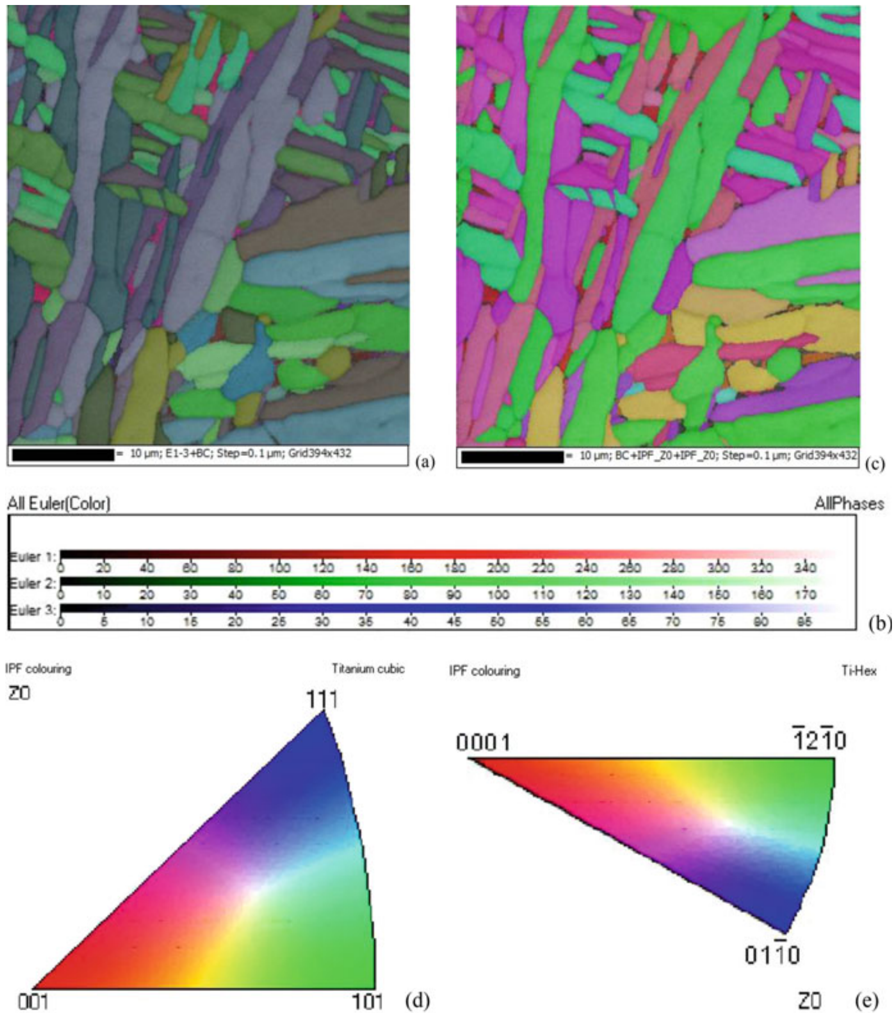

Fig. 5.22 (**a**) Euler map obtained from the Ti alloy specimen. Colors in this map represent the specific orientation of phases as shown in the orientation color key in (**b**). (**c**) Example of IPF coloring of the same specimen. Legend of IPF map for (**d**) cubic and (**e**) hexagonal Ti

boundaries can be investigated. Calculation of misorientation between each pixel reveals the sub-grain structure of a material.

EBSD can also be used to check if a material has a specific orientation (i.e., texture). In this method, crystal orientation measurements are made at multiple points within a phase, and the information is combined to conclude if the phase has texture. The orientation data can be displayed in a "Euler" map (see Fig. 5.22a, b). Generation of such maps is useful since they make it easy to visualize the distribution of texture within a specimen. Inverse pole figure (IPF) maps (see Fig. 5.22c–e) are also used

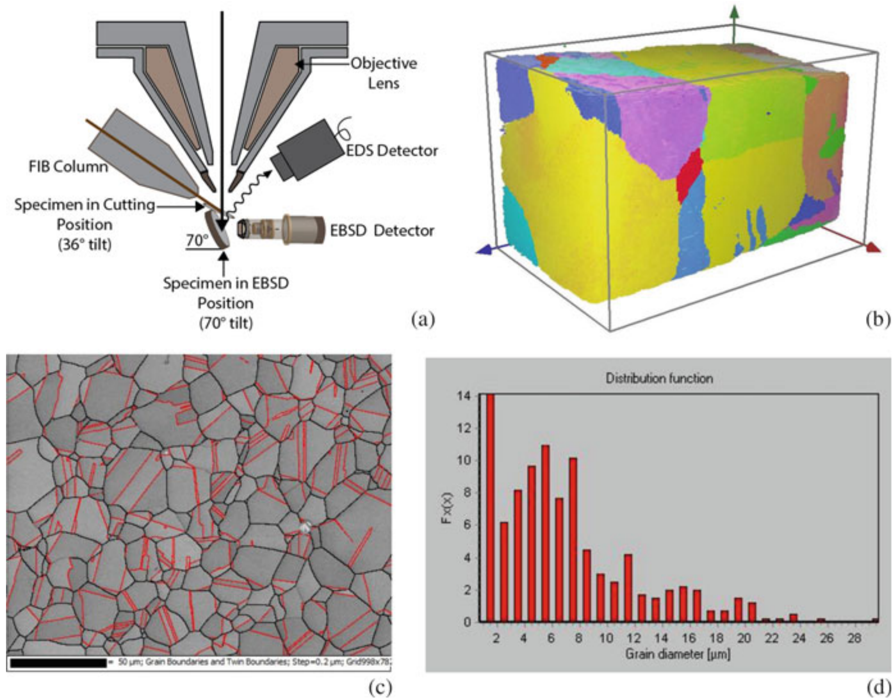

Fig. 5.23 (**a**) Experimental setup depicting the combined use of EBSD and FIB in an SEM. (**b**) 3-D EBSD orientation map of annealed copper wire. (**c**) Grain boundaries from a stainless steel sample determined by EBSD. It highlights the grain boundaries (black) and twin boundaries (red) distribution in the steel. (**d**) Grain size distribution of stainless steel sample

to show 3-D texture on a 2-D plane by converting crystallographic directions into points.

EBSD and EDS can be integrated to acquire simultaneous crystallographic and compositional data, respectively, from each analyzed point in a synchronized manner. Microchemical analysis results obtained using EDS can be used to shortlist candidate phases based on composition. The shortened list is then used to index the EBSD pattern. For a material with known phases, the distribution and fraction of phases can be determined using EBSD. Combined EDS and EBSD technique is helpful during mapping to separate phases that possess similar crystal structure.

EBSD combined with focused ion beam (FIB) instrument (see Fig. 5.23a) has enabled scientists to acquire 3-D microstructural information from specimen volume. In this automated process, milling is used to expose fresh surface within a volume to acquire an EBSD map. The series of maps obtained at increasing depths of the specimen are later combined to generate a three-dimensional microstructure of the analyzed specimen volume (see Fig. 5.23b). Examples of grain boundary structure and grain size distribution obtained using EBSD are shown in Fig. 5.23c, d, respectively.

The design of EBSD detectors has been continuously improved to meet the challenges presented by nanomaterials which require low accelerating voltage, small probe current, and short working distance during analysis. These conditions generate low-intensity diffraction signals, and sensitive detectors had to be designed to detect them within reasonable acquisition time.

EBSD technique has evolved in terms of automated accuracy along with the increase in the speed of analysis and data acquisition. This improvement has reached to an extent that today the ability of the incident beam to scan multiple points and thus create a map representing the orientation of grains of the scanned area is the most common method of evaluating material microstructure. An orientation map (OM) is distinct because of its locality and scope and by the sampling period between points. Hence, resolution of OM can be accustomed to exposing the structure of grains and character of the grain boundary. Over the years, the development in the speed of analysis has made a shift from a point where indexing was done manually to a point where now 100 patterns could be indexed per second automatically. Time of indexing/analysis is few tens of seconds, and precision of angular measurement is close to 0.5°. The spatial resolution of 20–100 nm is possible if the EBSD detector is coupled to a FESEM. Improved resolution of 10 nm has been demonstrated by using electron-transparent specimens with conventional EBSD hardware. This technique is referred to as transmission EBSD (t-EBSD) [32] or transmission Kikuchi diffraction (TKD) [33]. Improvement in spatial resolution is obtained by reducing the volume within the specimen from where the pattern is generated.

5.6 Electron Beam Lithography

5.6.1 Introduction

Semiconductor device fabrication is based on a sequence of photographic and chemical processes to manufacture structures at the micro- and nanoscale. The photographic process is known as lithography, a word that originates from the Greeks words *lithos*, meaning “stone,” and the word *grapho*, meaning “to write” [34]. Accurately translated as “writing on stone,” the technique of lithographic printing, from the late eighteenth century, used a flat stone slab onto which fat or oil was applied to split the slab into hydrophobic and hydrophilic regions. The ink applied to the slab would obey to only the hydrophilic regions, and when the paper was contacted with the slab, the ink would transfer to the paper making a copy of the hydrophilic regions on the slab. In lithography of semiconductor device fabrication, the “stone” is known as a mask and contains the pattern, and the “paper” used for printing the pattern is called substrate.

The substrate can be made from any material that can be formed into a flat plate, for example, Si, GaAs, and Quartz, among others, are widely used. The substrate material is often selected due to its electrical or thermal properties which may allow specific types of semiconductor devices to be realized. To write on these substrates,

many lithographic-based techniques could be used. The most common techniques are imprint lithography, optical lithography, and electron beam lithography. The illumination source is used in optical lithography; this source is projected through the mask that contains the wanted pattern. Imprint lithography is based on the molding process, in which a deformable layer placed on the substrate surface could be structured directly. In electron beam lithography, an accelerated electron beam is used on the substrate surface placed on a movable stage. That stage moves the sample carefully so that the electron beam can scan across the whole substrate surface to trace the desired pattern.

None of these processes directly affect the surface of the substrate, so to allow the pattern to be transferred into the substrate, a thin layer of *resist* is used. In the case of electron beam lithography, the resist layer is sensitive to photons or electrons. This sensitivity results in a change in chemical properties of the resist at the points where it has been exposed to the radiation source, resulting in a change in dissolution rate in a given solvent which allows the pattern to be formed in the resist layer. Electron beam lithography is the gold standard in terms of being able to produce the highest-resolution features; however, its extremely low throughput precludes its use in large-scale industrial manufacturing. The high resolution and flexibility of electron beam lithography have ensured that it has a particular role in research and development applications. A good overview of the technique is written by Nabity et al. [35].

5.6.2 Experimental Set-Up

Electron beam lithography has been used since the 1950s and can be performed on a wide spectrum of hardware from converted scanning electron microscopes, through to sophisticated commercial tools engineered expressly to provide the ultimate performance. A schematic diagram of the electron beam lithography system is shown in Fig. 5.24. The key systems are the cathode (cold or Schottky field emitter) where electrons are generated, the electromagnetic lenses and scan coils which focus the electron beam and provide a method to control the deflection of the beam across the substrate, and *X*-*Y*-*Z* stage on which the substrate coated with resist is mounted, along with the vacuum, electronic control, and power supply systems. Dedicated E-beam control unit is provided, which contains a pattern generation system to convert computer-aided designed patterns into control signals for the beam deflection and blanking system. Converted SEM may have an external pattern generator system. More advanced tools may also contain a substrate handling system allowing multiple substrates to be automatically loaded and unloaded from the machine for exposure in a sequential or “batch” fashion. The entire machine may be mounted on a plinth and/or contain a vibration isolation table, which stabilizes the system reducing effects of seismic activity and isolating the equipment from environmental sources of mechanical vibration.

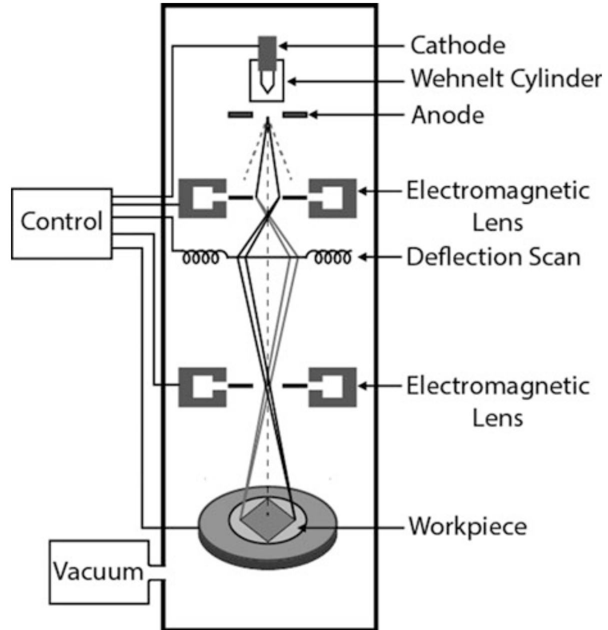

Fig. 5.24 Schematic representation of an electron beam lithography system [36]

5.6.3 Classification of E-beam Lithography Systems

Electron beam lithography systems can be classified on the basis of the beam shape and beam deflection method. An important distinction between different types of electron beam lithography tools is that of shaped-beam versus Gaussian-beam. With a Gaussian-beam system, the electron beam is focused down to have as small a diameter as the beam current will allow and the cross-sectional intensity profile of such a beam can be approximated by a Gaussian function. Shaped-beam systems form the electron beam into a wide beam of uniform intensity. This wide beam is then passed through a series of interchangeable apertures which allow the beam to be directly formed into trapezium shapes. In this way, while with a Gaussian-beam system, each shape is formed from a series of point exposures, in a shaped-beam system, each shape can be exposed as one "shot" or exposure. As a result, throughput is vastly superior with shaped-beam systems when large patterns are exposed. However, this comes at the cost of ultimate resolution. Shaped-beam systems have found significant use in advanced manufacturing facilities, but their relative expense compared with Gaussian-beam systems and their slightly lower-resolution capabilities mean that Gaussian-beam systems are of more interest in a university research setting [37–39].

5.6.4 Working Principle

5.6.4.1 Beam Deflection and Blanking

In electron beam lithography, two strategies are used to control the beam deflection and blanking: raster scanning and vector scanning. With raster scanning, the beam is scanned in a series of parallel scan lines across the complete subfield, and the beam blanker is switched on and off to control which parts are written. In a vector scan system, the beam is deflected to the start of each shape to be written and then scanned across that shape, before being deflected to the start of the next shape. It means that the beam is on for a much greater proportion of the writing time since it is only blanked when moving between shapes. Both tools are ultimately limited by the brightness of the electron source.

5.6.4.2 Pattern Design and Electron Beam Resist

The whole aim of lithography is to form a pre-defined pattern on a physical object. To create the pattern in the first place, it is extremely common to use a form of computer-aided design (CAD) to create an electronic file containing the required arrangement of shapes. All conventional forms of lithography rely on the use of a layer of resist, which is a layer of material which can be selectively removed so that it protects some areas of the substrate and exposes other areas to subsequent processing, for example, etching. In electron beam lithography, the resist is formed from a compound that undergoes chemical changes when exposed to energetic electrons. There are two forms that these changes can take, and this determines the type of resist, positive or negative [40]. When electrons interact with a "positive" resist, they cause scissions in the polymer chains that make up the resist. This makes the exposed regions more soluble in a chemical solution known as a developer. With negative resist, the incident electrons cause the molecular chains to cross-link [41]. This makes the exposed regions less soluble in the developer. The illustration in Fig. 5.25 shows the final resist profile for both positive and negative resists.

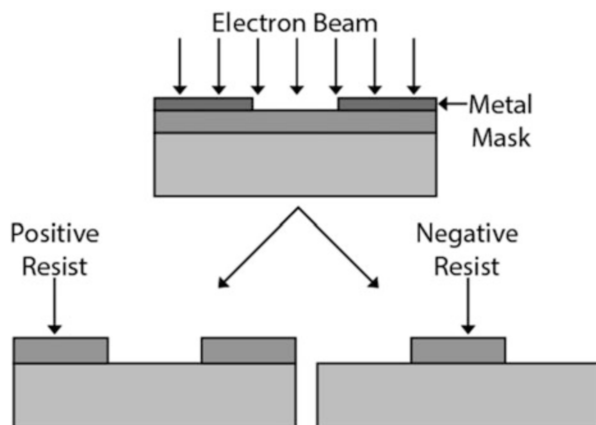

Fig. 5.25 Diagram showing the differences in the final resist profile for positive and negative resist exposed to the same electron beam pattern [42]

The degree of change caused by the electrons impacting on the resist is affected by the number of electrons or the electron dose, and on the accelerating voltage, since this controls the production of secondary electrons which actually expose the resist. Similarly, the rate of dissolution and the difference in final resist thickness can be controlled by changing the concentration of the developer and the amount of time used for development. In this way, a set of process parameters sometimes referred to simply as a "process," can be defined to give well-defined features. In general, there exists two commonly used E-beam resists; polymethyl methacrylate (PMMA) and hydrogen silsequioxane (HSQ). PMMA has been used as a resist for electron beam lithography for nearly 40 years [43]. It is a positive resist at moderate electron dose, but it can also be used as a negative resist at much higher electron dose [44].

5.6.4.3 Pattern Processing

There are two main fabrication processes used frequently in small-scale semiconductor fabrication. The processes can be thought of as roughly inverse of each other as one of the processes is an additive process, "lift-off," with the other is a subtractive process, "etching." Lift-off allows the patterned metal to be added to a substrate. It relies on the resist having an undercut profile after development such that the top of the features in the resist are slightly narrower than the bottom. The undercut resist profile means that when a thin layer of metal is deposited on top of the whole substrate, the metal becomes discontinuous at all the edges of the pattern. Submerging the substrate in a solution which dissolves the resist removes the remaining resist along with any metal on top of it, resulting in a metal layer attached to the substrate that matches the pattern of the electron beam exposure. This process is illustrated in Fig. 5.26a. A pattern produced by E-beam lithography is shown in Fig. 5.26b.

The metal can be deposited in a number of ways: filament evaporation, electron beam evaporation, effusion cell evaporation, and laser ablation. Sputter-coated metal generally cannot be used for a lift-off process.

Etching is the second method of pattern transfer and it is a subtractive method. Starting with a blank substrate, a blanket deposition of metal is performed. The resist is coated onto the metalized substrate, and lithography is then performed. After development, the substrate has regions where the underlying metal surface is exposed and regions still coated with a resist. The exposed metal regions are then removed in an etchant, while the resist protects and prevents the removal of the covered metal regions. The etchant used can be either a chemical solution, in which case the process is known as "wet etching," or it could be a gas or plasma etchant, in which case the process is called "dry etching."

5.6.5 Applications

Because of its flexibility, E-beam lithography is the most commonly used method for precise patterning in nanotechnology applications. Generally, it could be used in the nanoelectromechanical system (NEMS), quantum structures, magnetic devices,

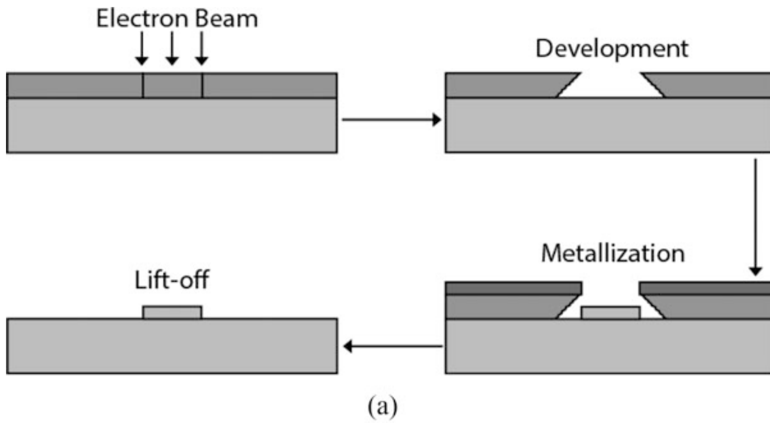

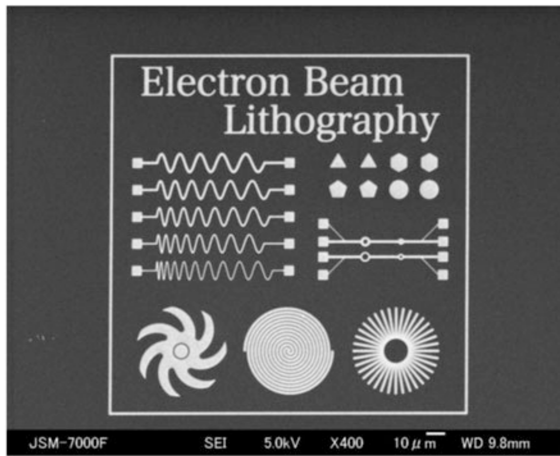

Fig. 5.26 (**a**) Schematic representation of a lift-off process for transferring the pattern [36]. (**b**) SEM image of a pattern produced using E-beam lithography. (Image courtesy of T. Siong, JEOL Ltd.)

solid-state physics, biotechnology, and transport mechanisms. It is used in the fabrication of many functional devices and products such as IC fabrication mask, nano-transistors, nano-sensors, and biological applications such as biomolecular motor-powered devices.

5.7 Electron Beam-Induced Deposition (EBID)

5.7.1 Mechanism

In electron beam-induced deposition (EBID), gaseous molecules are decomposed by an electron beam resulting in the deposition of nonvolatile fragments onto a substrate. The electron beam is typically provided by the SEM. Using this technique, free-standing 3-D structures are generated at high spatial resolution. The electron beam interacts with the material resulting in the emission of secondary electrons which in turn decompose molecular bonds of precursor gaseous materials resulting in deposition. The mechanism of dissociation is complex because it involves a large number of excitations in the close neighborhood of the substrate. Due to these complexities, there is no analytical solution for this technique; only gross approximations are available.

The precursor used for deposition can be solid, liquid, or gas. Liquids and solids need to be converted into gas form prior to deposition. The gas is introduced at the surface of the substrate in a controlled fashion, and electron beam is scanned in the desired manner to deposit the material in the required shape and size. In this way, materials can be deposited with a high spatial resolution of 1 nm. This can be useful in the electronics industry where nanoscaled structures are required. A range of materials can be deposited including Au, amorphous C, diamond, Si_3N_4, W, Pt, Pd, GaN, and many other elements. The deposits are clean and can be characterized in situ in the microscope.

If the focused ion beam is used to deposit materials, the process is termed ion beam-induced deposition (IBID). In this case, heavy gallium ions are used for deposition. The deposition process is similar to that in EBID with a lower spatial resolution due to the wider angular spread of secondary electrons. The deposition rate is higher due to heavier ions, but at the same time, the contamination rate increases due to the same reason. Mostly, such a deposition is undertaken in an instrument that combines FIB with FE-SEM. Free standing three-dimensional structures can be deposited with these techniques including nano-wires, nano-loops, nano-trees, etc.

A specially designed chamber is used because temperature rises during deposition. The chamber is isolated from the column, and beam comes in through a small hole in it. A general schematic of EBID technique is as shown in the Fig. 5.27.

It can be seen in Fig. 5.27 that the precursor gas comes into the chamber from the left-hand side of the substrate. A high-energy electron beam comes in and hits the precursor material placed on top of the substrate. During this process, multiple excitations take place and volatile part of the gas moves away. Only the nonvolatile part is left behind. In this way, once the precursor gas is led into the chamber, the electron beam scans over the substrate and deposits a layer of the precursor on the substrate. The scanning is controlled by a computer system. The rate and quality of deposition depend on the various factors such as pressure, the temperature of the material, and characteristics of the electron beam.

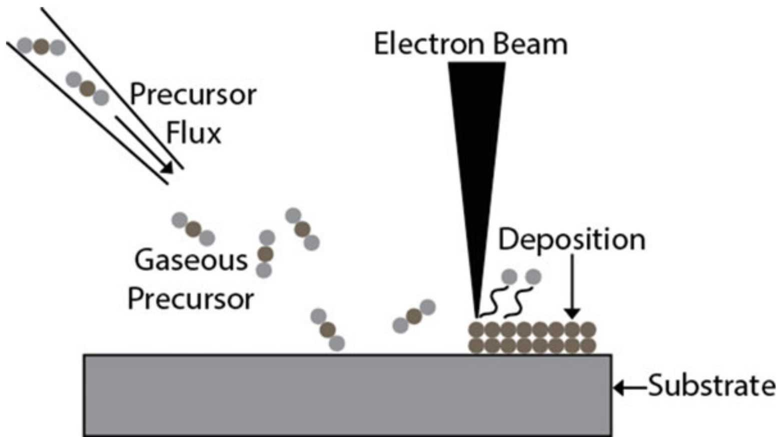

Fig. 5.27 Schematic diagram of electron beam-induced deposition

5.7.2 Advantages/Disadvantages of EBID

Advantages

1. This technique is very flexible with regard to the composition of the deposited material and its shape. Both of these factors are computer controlled.
2. The size control of the product after deposition and the accuracy of the process are high.
3. The characterization and deposition can be done simultaneously.

Disadvantages

1. It is a challenge to accurately control the chemical composition of the deposited material.
2. The structure broadening may happen due to proximity factors.
3. In the case of serial deposition, the rate of deposition is slow.

5.7.3 Applications

EBID is used to characterize, analyze, and fabricate nanomaterials and devices. The EBID structure can be developed using two separate gas injection systems (GIS) that introduces carbon and platinum precursor into the system. This is used as a hard mask in the production of quantum cellular automata (QCA) device structures [45]. Another application is the production of atomic force microscopy (AFM) cantilevers using EBID. If such a tip is produced in a cylindrical shape, it will lessen the effect of forces of attraction between specimen and probe during AFM. Carbon nanotubes have been attached to produce an ultra-sharp tip with radius from 6 to 25 nm using EBID on damaged AFM tips. A structure produced by EBID technique is shown in Fig. 5.28.

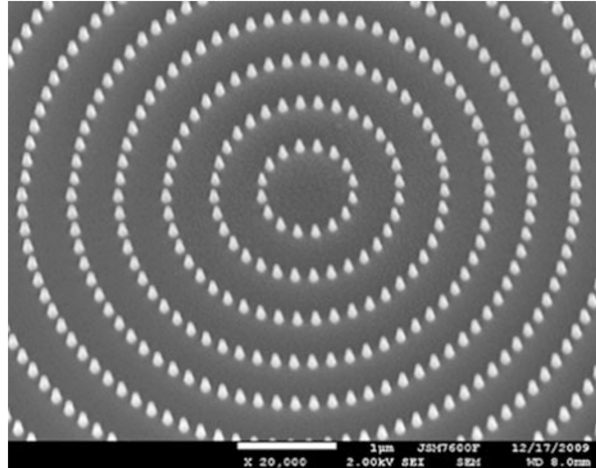

Fig. 5.28 SEM image of a structure produced by EBID: Pt nanodots deposited on Si wafer. (Image courtesy of T. Siong, JEOL Ltd.)

5.8 Cathodoluminescence

5.8.1 Introduction

A particular class of materials can emit light (photons of characteristic wavelengths in ultraviolet, visible, and infrared ranges) when bombarded with an electron beam in the SEM. This phenomenon is known as cathodoluminescence (CL) which occurs when atoms in a material excited by high-energy electrons in the beam return to their ground state, thus emitting light. Examples of cathodoluminescence from everyday life are light emitted from the inner surfaces of the cathode ray tubes in television set or computer monitors.

Cathodoluminescence can be observed with a special detector mounted in the SEM column. The detector collects the light or the wavelength emitted by the specimen. It can display the real color of visible light or an emission spectrum. Examples of materials that exhibit cathodoluminescence include zinc sulfide, anthracene, sedimentary rocks, semiconductors, Si wafers, synthetic crystals, fluorescent dyes, etc. Cathodoluminescence provides information about the distribution of trace elements in minerals, impurities in ceramics, and defects in crystals, etc. Some materials like plastics and glasses also show weak cathodoluminescence emission. This technique has found an important place in the microelectronics industry. It is used to study the optical and electronic properties of semiconductor materials. Semiconductors are bombarded with high-energy electron beam which transfers its energy into electrons that jump from valence into conduction band leaving behind holes. Recombination of electron holes at p-n junctions results in cathodoluminescence. In this manner, nanoscale features and defects of semiconductors can be studied.

Cathodoluminescence microscopy has become an essential tool in the petrographic description of sedimentary rocks. CL also has important applications in igneous-metamorphic petrography, ore deposits, and mineralogy [46]. When electron beam hits the sample, it absorbs most of the incoming energy, and atoms of the specimen get excited. Normally, the excited atoms (also termed cathodoluminescent centers) return to the ground state by transfer of the excess energy to adjacent atoms by inelastic collisions. Under certain circumstances, the absorbed energy is re-emitted as light energy in the visible range before these collisions can take place. The intensity of the light emitted from any particular point will be proportional primarily to the surface density of luminescent centers. The electron energy is readily absorbed in the sample, and little luminescence is emitted from below the surface. Transition metals and the rare earth elements are particularly susceptible to electron beam excitation. For instance, in transition metals, the 3-D electron shells are available for excited electrons to enter these levels. Thin sections, rock slabs, and loose grains can all be examined in the CL stage. Fine grains should be cemented to a glass slide so they will not enter the vacuum system. Thick samples are restricted to $50 \times 70 \times 17$ mm. The view area in both cases is 50×70 mm.

5.8.2 Instrumentation

Most of the parameters in SEM-CL are same as that in normal SEM. The electrons are generated and then accelerated toward the anode by providing a potential difference of 1–30 kV. The current on the surface of the sample can vary from 1 pA to 10 nA. The working distance can be in the range of 4–40 mm. The electron beam is focused to (5 nm to 1 μm) probe that can produce a CL image of that small area. The CL detector is placed in the chamber at an angle to the specimen as shown in Fig. 5.29.

A large surface area of the sample is scanned by the electron beam and CL image is produced. The SEM-CL detector works under high vacuum 10^{-4} Pa and is capable of producing high-resolution images. This image is just like a digital image showing different colors. The magnification of the CL-images can range from 10 to 10,000×, but it is difficult to obtain the lowest magnification due to instrumental configuration factors. The imaging process varies depending on the type of information that is required. The imaging process includes the CL (gray level image) in the range of ~200–800 nm. CL is frequently used to study the texture and chemical zone of the specimen. Three separate gray-colored images are obtained by using red, blue, and green color filters. Later, the image is recreated by using true colors. The *live* color image of the sample can be obtained by using an array detector system. A CL-SEM image is shown in Fig. 5.30.

Figure 5.31 shows various examples of CL images.

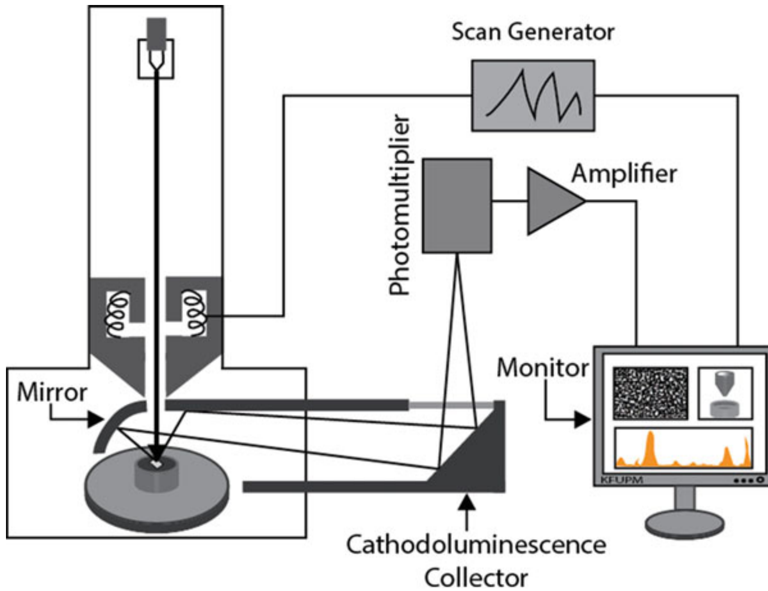

Fig. 5.29 Schematic showing the arrangement of cathodoluminescence detection in the SEM. The signal generated from the sample is reflected from the mirror into the CL detector and onto a photomultiplier tube for further processing

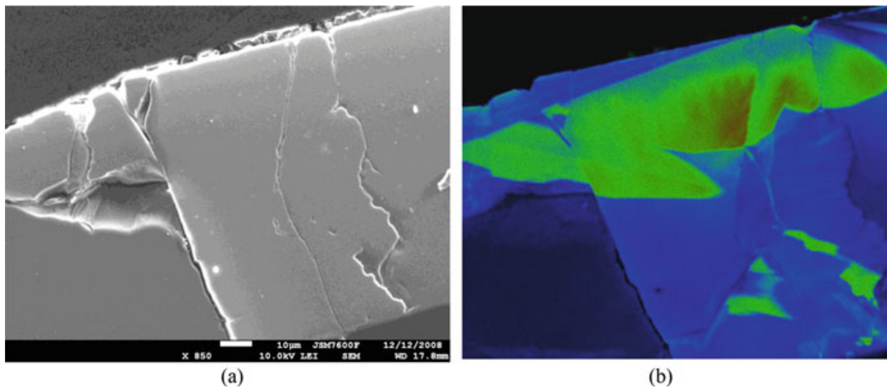

Fig. 5.30 SEM images showing cathodoluminescence of benitoite. (**a**) SEM image and (**b**) CL image. (Images courtesy of T. Siong, JEOL Ltd.)

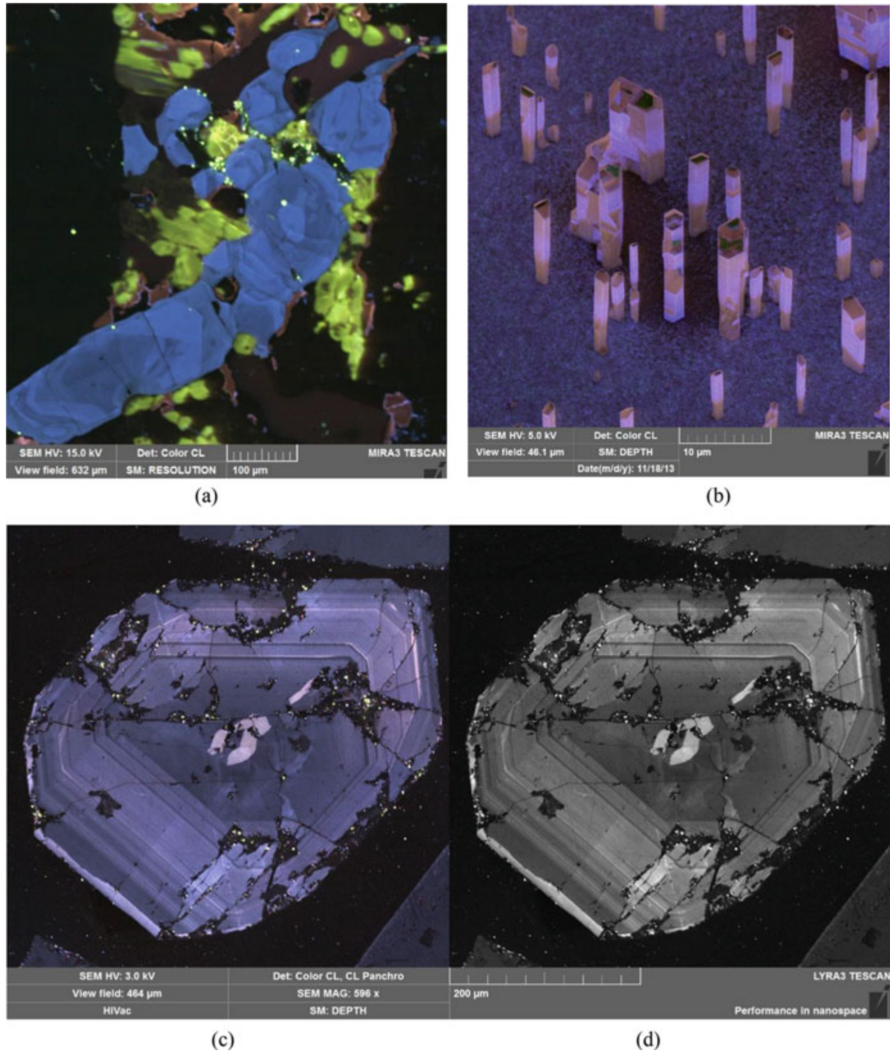

Fig. 5.31 CL images of (**a**) apatite and sodalite, (**b**) GaN wires with InGaN quantum wells and (**c**) zircon. (**d**) SEM image of zircon. (Images courtesy of TESCAN)

5.8.3 Strengths and Limitations of SEM-CL

The advantages of SEM-CL compared to optical-CL are the following:

- Spatial resolution is better.
- UV and IR response can also be obtained.
- Colorful image of the sample is created by using appropriate filters.

Some of the drawbacks of SEM-CL are the following:

- Complete setup with electron gun is required.
- The whole setup is more expensive than optical CL.
- The sample requires a conductive coating.
- Abnormalities in RGB color absorption filters and difficulties in proper color restoration.
- Difficult to obtain CL imaging of important CL-emitting minerals such as carbonate minerals and apatite.

5.8.4 Applications

The presence of trace elements in minerals can be detected using CL imaging. From different color patterns obtained from geological samples, the presence of trace elements can be confirmed. Some of the applications are as follows:

- CL imaging is very helpful in petrographic studies. For example, in clay cement, the bright blue luminescence indicates the presence of kaolinite [46].
- The zone analysis within the crystal can be done with CL imaging.
- Examination of cementation and diagenesis processes in sedimentary rocks can be undertaken [47].
- CL imaging is useful in studying the internal structure of fossils.
- Growth/dissolution analysis and deformation feature analysis in metamorphic minerals can be performed.
- With the help of this technique, various generations of the same minerals can be differentiated on the basis of trace amounts of activator elements. For example, sandstone can have many different types of quartz grains and compounds. Each different compound produces its own color pattern (different CL signal). These types of signals are invisible in secondary electron or backscattered imaging.

References

1. Boersch H (1954) Experimentale bestimmung der energieverteilung in thermisch ausgleoesten elektronenstrahlen. Z Phys 139:115
2. Erdman N, Bell DC (2013) SEM instrumentation developments for low kV imaging and microanalysis. In: Low voltage electron microscopy: principles and applications. Wiley, Chichester
3. Erdman N, Bell DC (2015) Scanning electron and ion microscopy of nanostructures. In: Kirkland AI, Haigh SJ (eds) Nanocharacterisation, RSC Nanoscience & Nanotechnology No. 37, 2nd edn. The Royal Society of Chemistry, Cambridge, p 311
4. Joens S (2001) Hitachi S-4700 ExB filter design and applications. Microsc Microanal 7:878–879

5. Sato M, Todokoro H, Kageyama K (1993) A snorkel type conical objective lens with E X B field for detecting secondary electrons. Proc. SPIE – Charged Particle Optics 2014:17–23
6. Kazumori H (2002) Development of JSM-7400 F: new secondary electron detection systems permit observation of non-conductive materials. JEOL News 37E(1):44–47
7. Steigerwald MDG, Arnold R, Bihr J, Drexel V, Jaksch H, Preikszas D, Vermeulen JP (2004) New detection system for Gemini. Microsc Microanal 10:1372–1373
8. Jaksch H (2008) Low Loss BSE imaging with the EsB Detection system on the Gemini Ultra FE-SEM. In: Luysberg M, Tillmann K, Weirich T (eds) Proceedings of EMC 2008, 14th European microscopy congress 1–5 September 2008, Aachen, Germany, vol 1. Springer-Verlag, Berlin Heidelberg, p 555 doi.org/10.1007/978-3-540-85226-1
9. Asahina S, Togashi T, Terasaki O, Takami S, Adschiri T, Shibata M, Erdman N (2012) High-resolution low-voltage scanning electron microscope study of nanostructured materials. Microsc Anal 26:S12–S14
10. Gestmann I, Kooijman K, Sakic A, Nanver L, van Veen G (2010) New solid state detector design for ultra-sensitive backscattered electron detection. In: Solorzano G, de Souza W (eds) Proceedings of the 17th international microscopy congress (IMC17), Rio de Janeiro, Brazil. International Federation of Societies for Microscopy (IFSM)
11. Sakic A, van Veen G, Kooijman K, Vogelsang P, Scholtes TLM, de Boer WB, Derakhshandeh J, Wien WHA, Milosavljevic S, Nanver LK (2012) High-efficiency silicon photodiode detector for sub-keV electron microscopy. IEEE Trans Electron Devices 59(10):2707–2714. https://doi.org/10.1109/TED.2012.2207960
12. Erdman N, Kikuchi N, Robertson V, Laudate T (2009) Multispectral imaging in a FEG-SEM. Adv Mat Proc 167(9):28–31
13. Schwandt CS (2010) Characterizing nanometer-scale materials using a low-angle backscattered electron detector. Amer Lab, Nov. 15, pp. 13–17
14. Mullerova I, Frank L (2003) Scanning low-energy electron microscopy. Adv Imag Elect Phys 128:309–443
15. Zach J (1989) Design of a high resolution low voltage scanning electron microscope. Optik 83 (1):30–40
16. Zach J, Haider M (1995) Aberration correction in a low voltage SEM by a multipole corrector. Nucl Instrum Methods Phys Res A 363:316–325
17. Honda K, Takashima S (2003) Chromatic and spherical aberration correction in the LSI inspection scanning electron microscope. JEOL News 38(1):36–40
18. Uno S, Honda K, Nakamura N et al (2005) Aberration correction and its automatic control in scanning electron microscopes. Optik 116:438–448
19. Kawasaki T, Tomonori N, Kotoko H (2009) Developing an aberration-corrected Schottky emission SEM and method for measuring aberration. Microelectr Eng 86:1017–1020
20. Kazumori H, Honda K, Matsuya M, Date M (2004) Field emission SEM with a spherical and chromatic aberration corrector. In: Proc. 8th Asian Pacific Conf. on Electr. Microsc. Council of Asia-Pacific Societies for Microscopy (CAPSM), pp 52–53
21. Thornley RFM (1960) Ph.D. thesis. University of Cambridge, Cambridge
22. Lane, WC (1970) Proceedings SEM Symposium (O. Johari, ed.), p. 43. IIT Research Institute, Chicago, IL
23. Danilatos GD (1988) Foundations of environmental scanning microscopy. Adv Electron Electron Phys 71:109–250
24. Johnson R (1996) Environmental scanning electron microscopy: an introduction to ESEM. Philips Electron Optics, Robert Johnson Associates, Eindhoven, The Netherlands
25. Melngailis J (2001) Ion sources for nanofabrication and high resolution lithography, proceedings of the 2001 particle accelerator conference, Chicago
26. Kikuchi S (1928) Diffraction of cathode rays by mica. Jpn J Phys 5:83–96
27. Boersch H (1937) Über Bänder bei Elektronenbeugung. Z Techn Phys 18:574–578
28. Alam MN, Blackman M, Pashley DW (1954) High-angle Kikuchi patterns. Proc R Soc Lond. Sect. A 221, pp. 224–242

29. Joy DC (1974) Electron channelling patterns in the scanning electron microscope. In: Holt DB, Muir MD, Boswarva IM, Grant PR (eds) Quantitative scanning electron microscopy. Academic Press, New York, pp 131–182
30. Biggin S, Dingley DJ (1977) A general method for locating the X-ray source point in Kossel diffraction. J Appl Crystallogr 10:376–385
31. Venables JA, Harland CJ (1973) Electron backscattering patterns. A new technique for obtaining crystallographic information in the scanning electron microscope. Philos Mag 27:1193–1200
32. Keller RR, Geiss RH (2012) Transmission EBSD from 10 nm domains in a scanning electron microscope. J Microsc 245(3):245–251
33. Trimby P (2012) Orientation mapping of nanostructured materials using transmission Kikuchi diffraction in the scanning electron microscope. Ultramicroscopy 120:16–24
34. Tallents G, Wagenaars E, Pert G (2010) Optical lithography: lithography at EUV wavelengths. Nat Photonics 4(12):809–811
35. Nabity J, Compbell L, Zhu M, Zhou W (2007) E-beam nanolithography integrated with scanning electron microscope. In: Zhou W, Wang ZL (eds) Scanning microscopy for nanotechnology, techniques and applications. Springer, New York, pp 120–151
36. Shwartz GC (2006) Handbook of semiconductor interconnection technology. CRC Press, Boca Raton
37. Pain L, Jurdit M, Todeschini J, Manakli S, Icard B, Minghetti B, Bervin G, Beverina A, Leverd F, Broekaart M, Gouraud P (2005) Electron beam direct write lithography flexibility for ASIC manufacturing: an opportunity for cost reduction (Keynote Paper). In: Emerging lithographic technologies IX, vol 5751. International Society for Optics and Photonics, pp 35–46
38. Pain L, Icard B, Manakli S, Todeschini J, Minghetti B, Wang V, Henry D (2006) Transitioning of direct e-beam write technology from research and development into production flow. Microelectron Eng 83(4):749–753
39. Todeschini J, Pain L, Manakli S, Icard B, Dejonghe V, Minghetti B, Jurdit M, Henry D, Wang V (2005) Electron beam direct write process development for sub 45nm CMOS manufacturing. In: Advances in resist technology and processing XXII, vol 5753. International Society for Optics and Photonics, pp 408–417
40. Zhou W, Wang ZL (eds) (2007) Scanning microscopy for nanotechnology: techniques and applications. Springer Science & Business Media, New York; London
41. Reichmanis E, Novembre AE (1993) Lithographic resist materials chemistry. Annu Rev Mater Sci 23(1):11–43
42. Chen YY, Chen CL, Lee PC, Ou MN (2011) Fabrication, characterization and thermal properties of nanowires. In: Nanowires-fundamental research. InTech, Rijeka
43. Hatzakis M (1969) Electron resists for microcircuit and mask production. J Electrochem Soc 116(7):1033–1037
44. Hoole ACF, Welland ME, Broers AN (1997) Negative PMMA as a high-resolution resist-the limits and possibilities. Semicond Sci Technol 12(9):1166
45. Bieber JA, Pulecio JF, Moreno WA (2008) Applications of electron beam induced deposition in nanofabrication. In: Proceedings of the 7th international Caribbean conference on devices, circuits and systems, ICCDCS http://ieeexplore.ieee.org/document/4542649/
46. Pagel M, Barbin V, Blanc P, Ohnenstetter D (2000) Cathodoluminescence in geosciences: an introduction. In: Cathodoluminescence Geosciences, vol 1995. Springer, Berlin, pp 1–21
47. Coenen T (2016) Cathodoluminescence imaging on sedimentary rocks: quartz sandstones, June, pp 1–14